Adaptive Motion Estimation and Control of Intelligent Walkers

by

Nursefa Zengin

A thesis
presented to the University of Waterloo
in fulfillment of the
thesis requirement for the degree of
Master of Applied Science
in
Mechanical Engineering

Waterloo, Ontario, Canada, 2015

I hereby declare that I am the sole author of this thesis. This is a true copy of the thesis, including any required final revisions, as accepted by my examiners.

I understand that my thesis may be made electronically available to the public.

Abstract

One of the most critical factors in the quality of elderly lives is their ability to move. As the size of the ageing society grows, more elderly people suffer from walking impairments. Most of them prefer to stay at home due to the shortage of the nursing care staff, since they deal with the daily challenges alone. Robotics researchers have developed various intelligent walking support systems to meet the needs of elderly and handicapped people. A particular problem in path tracking for such systems is maintaining the tracking performance, which is affected by the center of gravity (CG) shifts and load changes due to human-walker interactions. This thesis focuses on design of feedback controllers for safe motion of intelligent walker (i-walker) systems robust to CG shifts and load changes. Our design follows a two level approach, one for kinematics, the other for dynamics. The high level kinematic controller is designed based on integrator backstepping to produce desired velocities required for trajectory tracking. The low level dynamic controller is composed of a feedback linearization unit and a linear feedback controller to apply the control torque for tracking the desired velocity produced by the high level kinematic controller. As dynamic controllers, proportional-derivative (PD) and sliding mode controllers (SMCs) are designed. In our initial design, we assume that all system states are available. However, in the actual case, even if the wheel velocities can be measured with some sensor devices like tachometers, the measurements carry noise, which poses important problems in control algorithms. To obtain the estimates of the wheel velocities, avoiding the noise problems, the design of sliding mode observers and high gain observers is studied. The state feedback PD and SMC schemes are later integrated with these observers to form implementable output feedback controllers. In practice, the human mass and the distance due to the CG shift depend on the user. To address this issue, the output feedback control designs are further made adaptive, integrating with a parameter identifier to estimate these variables. The parameter identifier design involves a linear parametric model of the i-walker system dynamics and a least-square adaptive law based on this parametric model. Adaptive versions of the above observers and control designs are done utilizing estimated parameters and states. The effectiveness and applicability of the proposed controllers are verified via various simulations in MATLAB/Simulink environment.

Acknowledgements

I would like to thank my supervisor Prof. Baris Fidan for giving me opportunity to write my thesis in University of Waterloo and for his patience and educational support in every step of this work. I would like to also thank Prof. Dana Kulic and Prof. James Tung, my thesis committee, for giving me guidance and useful comments.

I would like to thank from all my heart to my precious family; mom, dad and my siblings; without their prays and their faith in me, I would not find myself. I also want to send my deepest love and thanks to my husband for his kindly help, patience and suggestions to improve my study.

Lastly, a special thanks to my real friends who have been with me in my tough times and believed in me during my journey.

Dedication

This is dedicated to all my family.

Table of Contents

List of Figures

List of Acronyms

CG Center of Gravity

HGO High Gain Observer

I-walker Intelligent Walker

MIMO Multi Input Multi Output

PD Proportional Derivative

SISO Single Input Single Output

SMC Sliding Mode Control

SMO Sliding Mode Observer

Chapter 1

Introduction

The population in many societies worldwide is getting older and age related impairments in physical ability make living independently challenging for elderly people. As an important class of such elderly people needing assistance, those with moving disabilities mostly need assistance to move and to maintain their balance [1].

Over the past decades, many robotic devices have been developed to enhance independent living for elderly. One of the most common assistive robotic devices is intelligent walker (i-walker) that helps elderly and handicapped people move independently. Its operation is easy and there is no need for detailed training to use it. The main issue for such systems is safe i-walker human motion which is generally hard to achieve due to inexact torque generation since the applied force by human on the i-walker has not been considered. The applied force on the handles must be taken into account in the i-walker dynamics for a safe walking. This extra load on the i-walker could be regarded as extra mass, called human effect [2]. The amount of this force is highly dependent on the user weight and body pose. Thus, the controller must be designed as robust to the these factors.

This thesis includes a two-part control problem regarding the safety and high performance. For the safe motion of i-walker systems, feedback controllers are designed considering center of gravity (CG) shifts and load changes. Integrator backstepping based high level kinematic controller is designed to produce the desired velocities of the i-walker system for trajectory tracking. Then, a low level dynamic controller is designed which con-

sists of a feedback linearization part and a linear feedback controller to apply the control torques for tracking the desired velocities produced by the high level kinematic controller. Proportional-derivative (PD) control and sliding mode control (SMC) schemes are implemented to the i-walker system as our dynamic controllers.

In order to implement feedback control laws, the i-walker wheel velocities are assumed to be known. Even though the wheel velocities of i-walker can be measured, this measurement contains noise which affects control performance. To reduce the noise and to achieve high performance, observers are designed to estimate velocities using two different approaches, in the form of sliding mode observer (SMO) and high gain observer (HGO). To form output-feedback controllers, the state feedback PD control and SMC designs are integrated with these observers producing estimates of i-walker wheel velocities.

The mass of support frame with human and CG shift are, in practice, unknown since they depend on the user. A parameter identifier is integrated to the system to estimate these values. First, a parametric model is built, then estimation model and estimation error are defined. A least-square adaptive law is designed based on this model and is applied to the system. Utilizing the estimated states and estimated parameters, adaptive versions of PD controller and SMC are designed.

The thesis is organized as follows. In Chapter 2, background information is presented to well-define the systems problem of interest and well-pose the relationship between the previous studies and our study. Description of the i-walker and detailed expression of the main problem are given. Additionally, dynamic model of the i-walker is introduced in Chapter 2. The control design for path tracking problem is firstly done in state-feedback form in Chapter 3. Simulation results are demonstrated to verify the validity of the proposed controllers. Chapter 4 presents two kinds of observers for state estimation and designs output feedback controllers related to state estimates. The observers are integrated to the state feedback control schemes to design output feedback PD and SMC schemes. To see the effectiveness of proposed observers and controllers, simulation results are shown as well. Parameter uncertainties due to the center of gravity shifts and load changes are considered, and accordingly parameter identification and adaptive control redesign are studied in Chapter 5. Finally, conclusions and future work directions are given in Chapter 6.

Chapter 2

Background and Modelling

2.1 Literature Review

Many people who suffer from visual, mobility impairments, and age related disabilities need to be assisted. Assistive robotics is a substantial part of life for people with disabilities to give them opportunities in terms of self motivation and independence in daily tasks. Aiming to help them, significant amount of research has been conducted for development of human assistive robotics technologies, including mobility focused ones.

For human mobility technologies, safety and efficiency are two main goals. Robotics researchers have conducted research on different kinds of intelligent devices such as canes, wheelchairs, omni-directional walkers, mobile robots, and i-walkers for developing control algorithms to deal with them [3–6].

Control algorithms that have been used in recent studies about assistive robotics are shown in Fig. 2.1. Shared control algorithm is used to control the system based on both the user and the walker according to the user's performance in [7, 8]. Collaborative control is designed to understand the user's intention, and adjust the control signals to achieve the user's target in [9]. An adaptive based motion control is used to prevent falls and to avoid collisions and obstacles in [10]. Model predictive control is used to minimize the difference between the reference position/velocity and the actual position/velocity in

[11]. An adaptive based motion control scheme is designed to attenuate the effects of the uncertainties due to the changes in the conditions of environment and the user in [12].

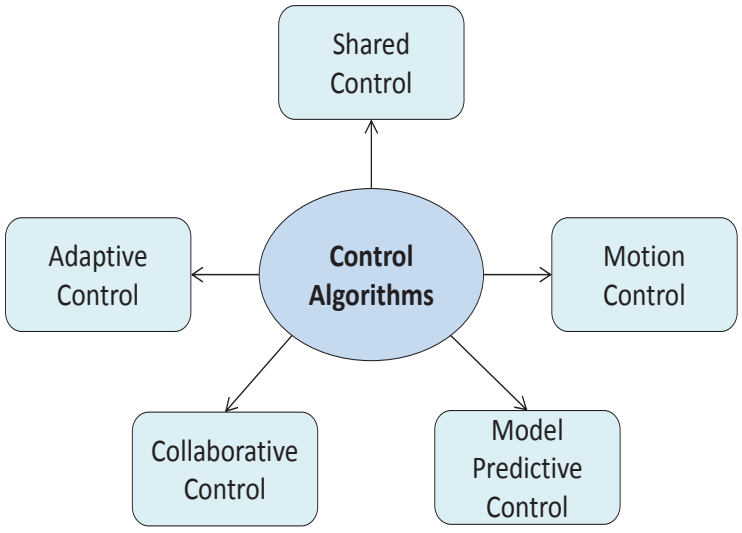

Figure 2.1: Control algorithms used in assistive technologies

I-walkers are mostly preferable because of their simple structures and benefits like being easy to use without any training. Based on their actuators, they are classified as active and passive type i-walkers. While the former type is heavy, complicated and costly, the latter is cost-efficient, compact in size, and intuitively easy to use [10]. Active type i-walkers contain servo motors to generate active motion of the system and sensors to obtain information about environment and user conditions. Unlike active ones, the passive i-walkers use servo brakes or servo motors for only steering based on user's intention. Passive walkers are often preferred because of simplicity and reliable behaviour [13].

In [14], a robot walking helper design is proposed based on combining active and passive control modes. A braking control law is used in passive control mode, whereas active one is considered to compensate for gravity if a user goes up a hill; and theory of differential flatness is used to plan the trajectory. In [15], a passive i-walker is controlled by only servo brakes for three states of the user; walking, emergency, and stopped states which

are detected using a laser range finder. In [16], two LQR controllers are designed to compute the optimal state feedback gain for the stabilization and balance enhancement of a two-wheeled i-walker. [17] has proposed an active omni-directional i-walker design that helps disabled people and focuses mainly on the user's intention, considering only indoor walking. In [18], an integrator backstepping method is proposed to stabilize the system at kinematic level transforming the original mobile robot system into a special chained form of nonholonomic system. However, none of above studies consider the dynamic effects such as CG shifts, load changes, friction, uncertainties. For a good tracking performance, these effects are also needed to be considered. In [19], an adaptive control design is presented for a certain dynamic walker model with omni-directional wheels to control the omnidirectional walker follow a path considering CG shifts. In [20], another adaptive controller is designed for walking support machine with mecanum wheels to solve the collision problems caused by both center of gravity shifts and load changes. All of the studies discussed can be applied to different types of walking support systems. In this thesis, active type i-walkers are considered to apply control techniques as a special class of walking support systems.

For most of the motion controllers, both wheel displacements and velocities of i-walker are needed to be known. Displacement and velocities can be measured by encoders and tachometers, respectively. However, the wheel velocity measurements in practical applications contain noise [21]. To eliminate the effects of measurement noise, some of the works on the i-walker motion control use state observers within the control loop to estimate the velocities.

Among various observer design approaches, in this thesis, sliding mode observers (SMOs) and high gain observers (HGOs) are taken into consideration. For different nonlinear systems, SMO is analysed to reduced the estimation error in [22]. [23] combines adaptive nonlinear controllers, and stability and performance bounds using different types of observers. [24] studies adaptive observers for SISO observable nonlinear systems that can be converted to observable canonical form. [25] has used the Lyapunov's direct method for formal design and analysis of adaptive observers. A new approach is presented in [26] to estimate the states of a robot manipulator by using nonlinear sliding mode observers. [27] also demonstrated a robust adaptive observer based on adaptive nonlinear damping for MIMO nonlinear systems with unknown parameters.

Chattering problem of SMOs has received a great deal of attention in most of these studies. SMO generates chattering which is the main drawback of this observer. Chattering is undesirable, since it has high frequency discontinuous components, which affects the control law. [28] presented how these undesirable high frequency dynamics can be used in control law to have a better solution.

HGOs have had an important place in literature. First appearance of HGOs was the end of 70s. [29] focused on one of the difficulties that can be solved by observers which is robustness. The development of high gain observers continued during 80s in H_∞ optimization of uncertain linear systems [30] and a high gain feedback stabilization in nonlinear systems [31]. Peaking phenomenon leads to problems when high gain observer is used in control systems. In order to diminish the effect of peaking, the non-linearities are analysed by [32]. In this thesis, state estimators are designed by taking the previous implementations into consideration and integrated to active type i-walker systems to estimate wheel velocities.

2.2 Structure and Modelling

The i-walker structure studied in this thesis consists of a support frame with battery, two driving wheels placed at the user side and two free casters placed on the front side. It is based on a commercial walker configuration shown in Fig. 2.2 [33].

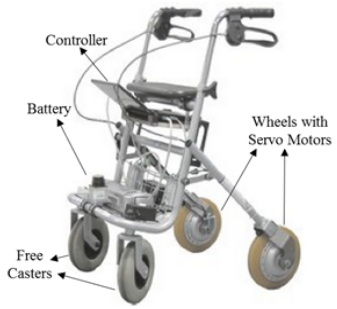

Figure 2.2: Intelligent Walker [33]

The geometric/kinematic model of a non-holonomic i-walker is illustrated in Fig. 2.3. It is assumed that the i-walker system moves on a flat plane. The system motion is represented in two different 2D coordinate systems that are the global coordinate system $\{X, Y\}$, with a certain fixed origin O, and the body fixed coordinate system $\{x, y\}$, with origin at the mid-point A on the axis between the rear wheels.

The i-walker is driven by two independent motors coupled with rear wheels whose radius are r. The distance between wheel centres is $2L$. The nominal position of CG at the i-walker system is assumed to be on the axis of symmetry, at a distance d from the origin A.

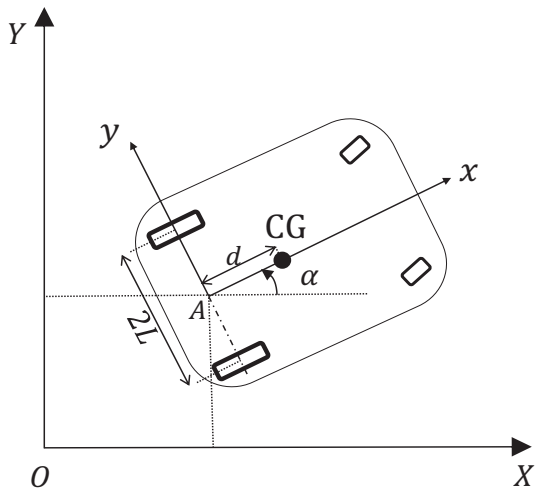

Figure 2.3: Model of i-walker system

The global state of the i-walker in the reference frame is specified by the vector $p = [x_A, y_A, \alpha]$ where (x_A, y_A) and α are the global coordinates of point A and the heading angle, respectively. The kinematic equations of the i-walker system is represented using a Jacobian matrix as follows:

$$\begin{bmatrix} \dot{x}_A \\ \dot{y}_A \\ \dot{\alpha} \end{bmatrix} = \begin{bmatrix} cos\alpha & 0 \\ sin\alpha & 0 \\ 0 & 1 \end{bmatrix} \begin{bmatrix} v_A \\ \omega_A \end{bmatrix}, \tag{2.1}$$

where v_A and ω_A are the linear and angular velocities, respectively, which can be written in the form

$$\begin{bmatrix} v_A \\ \omega_A \end{bmatrix} = R\dot{\eta}, \qquad \eta = \begin{bmatrix} \theta_R \\ \theta_L \end{bmatrix}, \quad R = \begin{bmatrix} \frac{r}{2} & \frac{r}{2} \\ \frac{r}{2L} & \frac{-r}{2L} \end{bmatrix}, \tag{2.2}$$

where θ_R and θ_L represent the rotational displacements of right and left powered rear wheels, respectively. The forward kinematic model is obtained by substituting (2.2) in (5.9):

$$\begin{bmatrix} \dot{x}_A \\ \dot{y}_A \\ \dot{\alpha} \end{bmatrix} = \begin{bmatrix} r\frac{cos\alpha}{2} & r\frac{cos\alpha}{2} \\ r\frac{sin\alpha}{2} & r\frac{sin\alpha}{2} \\ \frac{r}{2L} & \frac{-r}{2L} \end{bmatrix} \begin{bmatrix} \dot{\theta}_R \\ \dot{\theta}_L \end{bmatrix} = T\dot{\eta}, \tag{2.3}$$

where $T = \begin{bmatrix} r\frac{cos\alpha}{2} & r\frac{cos\alpha}{2} \\ r\frac{sin\alpha}{2} & r\frac{sin\alpha}{2} \\ \frac{r}{2L} & \frac{-r}{2L} \end{bmatrix}$. Introducing the generalized coordinate vector

$$q = \begin{bmatrix} x_A & y_A & \alpha & \theta_R & \theta_L \end{bmatrix}^T,$$

the constraint equation can be defined under the assumptions of pure rolling and no slipping as

$$A(q)\dot{q} = 0, \tag{2.4}$$

where the constraint matrix is

$$A(q) = \begin{bmatrix} -sin\alpha & cos\alpha & 0 & 0 & 0 \\ cos\alpha & sin\alpha & L & -r & 0 \\ cos\alpha & sin\alpha & -L & 0 & -r \end{bmatrix}.$$

Let $S(q)$ be a full rank matrix formed by a set of smooth and linearly independent vector fields spanning the null space of $A(q)$, which satisfies

$$S^T(q)A^T(q) = 0, \tag{2.5}$$

the kinematic equations of the point A are obtained as

$$\dot{q} = S(q)\dot{\eta}, \tag{2.6}$$

where

$$S(q) = \begin{bmatrix} \frac{r}{2}cos\alpha & \frac{r}{2}cos\alpha \\ \frac{r}{2}sin\alpha & \frac{r}{2}sin\alpha \\ \frac{r}{2L} & -\frac{r}{2L} \\ 1 & 0 \\ 0 & 1 \end{bmatrix}.$$

The total kinetic energy of the system is expressed in the following form:

$$T_{total} = \frac{1}{2}m\left(\dot{x}_A^2 + \dot{y}_A^2\right) - m_c d\dot{\alpha}\left(\dot{y}_A cos\alpha - \dot{x}_A sin\alpha\right) + \frac{1}{2}I_w\left(\dot{\theta}_R^2 + \dot{\theta}_L^2\right) + \frac{1}{2}I\dot{\alpha}^2, \tag{2.7}$$

$$\begin{aligned} m &= m_c + 2m_w, \\ I &= I_c + m_c d^2 + 2m_w L^2 + 2I_m, \\ \dot{\alpha} &= r\frac{(\dot{\theta}_R - \dot{\theta}_L)}{2L}, \end{aligned} \tag{2.8}$$

where m_c refers to the mass of the support frame with the mass from the partial body weight support of the user. m_w represents the mass of each driven wheel with a motor, I_c is the moment of inertia of the support frame about the vertical axis through the CG, I_w and I_m are the moment of inertia of each powered wheel with a motor about the wheel axis and the wheel diameter, respectively. The dynamic model of the i-walker can be written as follows:

$$M(q)\ddot{q} + C(q,\dot{q})\dot{q} = B(q)\tau - A^T(q)\lambda, \tag{2.9}$$

where λ is the vector of Lagrange multipliers, $M(q), C(q,\dot{q}), B(q)$, and τ are the symmetric positive definite inertia matrix, the centripetal and Coriolis matrix, the input matrix, and torque vector, respectively.

$$M(q) = \begin{bmatrix} m & 0 & m_c d sin\alpha & 0 & 0 \\ 0 & m & -m_c d cos\alpha & 0 & 0 \\ m_c d sin\alpha & -m_c d cos\alpha & I & 0 & 0 \\ 0 & 0 & 0 & I_w & 0 \\ 0 & 0 & 0 & 0 & I_w \end{bmatrix}, \quad \tau = \begin{bmatrix} \tau_R \\ \tau_L \end{bmatrix},$$

$$C(q,\dot{q}) = \begin{bmatrix} 0 & 0 & -m_c d\dot{\alpha} sin\alpha & 0 & 0 \\ 0 & 0 & -m_c d\dot{\alpha} cos\alpha & 0 & 0 \\ 0 & 0 & 0 & 0 & 0 \\ 0 & 0 & 0 & b_m & 0 \\ 0 & 0 & 0 & 0 & b_m \end{bmatrix}, \quad B(q) = \begin{bmatrix} 0 & 0 \\ 0 & 0 \\ 0 & 0 \\ 1 & 0 \\ 0 & 1 \end{bmatrix},$$

where b_m is the viscous damping on the motor. It should be noted that friction and gravity components are not included to simplify the equations.(2.9) can be rewritten in input-state form for convenience of control design and analysis by eliminating the constraint term $A^T(q)\lambda$ [35]. Substituting (2.6) in (2.9), and then multiplying both sides by $S^T(q)$, the reduced dynamic model is obtained as follows:

$$\bar{M}\ddot{\eta} + \bar{C}\dot{\eta} = \bar{B}\tau, \tag{2.10}$$

where

$$\bar{M} = S^T(q)M(q)S(q) = \begin{bmatrix} \frac{mr^2}{4} + \frac{Ir^2}{4L^2} + I_w & \frac{mr^2}{4} - \frac{Ir^2}{4L^2} \\ \frac{mr^2}{4} - \frac{Ir^2}{4L^2} & \frac{mr^2}{4} + \frac{Ir^2}{4L^2} + I_w \end{bmatrix},$$
$$\bar{C} = S^T(q)M(q)\dot{S}(q) + S^T(q)C(q,\dot{q})S(q) = \begin{bmatrix} b_m & m_c\frac{r^2d}{2L}\dot{\alpha} \\ -m_c\frac{r^2d}{2L}\dot{\alpha} & b_m \end{bmatrix}, \tag{2.11}$$
$$\bar{B} = S^T(q)B(q) = \begin{bmatrix} 1 & 0 \\ 0 & 1 \end{bmatrix}.$$

It should be noted that while obtaining dynamic model of the system, the CG shift in the x-direction is only considered. The dynamic model of the nonholonomic i-walker system has the following properties [36]:

Property 2.1. The inertia matrix $\bar{M}$ is symmetric positive definite, and hence satisfies the inequality

$$\lambda_{min}\left(\bar{M}\right) I \leq \bar{M} \leq \lambda_{max}\left(\bar{M}\right) I, \tag{2.12}$$

where $\lambda_{min}\left(\bar{M}\right)$ and $\lambda_{max}\left(\bar{M}\right)$ denote the minimum and the maximum eigenvalues of $\bar{M}$, respectively.

Property 2.2. The matrix $\dot{\bar{M}} - 2\bar{C}$ is skew-symmetric, and hence

$$x^T\left(\dot{\bar{M}} - 2\bar{C}\right)x = 0, \quad \forall x \epsilon \Re^{n-m} \tag{2.13}$$

2.3 Control Problem

Passive walkers are intrinsically safe but they increase the metabolic cost. Active walkers provide efficient walking; however, they are not safe due to the unintentional movement of the i-walker which could be result of inappropriate torque applied by independent motors. Many researchers have not considered human mass effect on the system dynamics. In this work, both human partial body weight and i-walker weight are taken into consideration to obtain (2.10). In this regard, a path tracking control problem is aimed by designing a

high level kinematic controller to produce the desired velocities, v_d and ω_d, and feedback linearizing system with dynamic controller to apply the control torque for tracking the desired velocities. PD control and SMC are designed as dynamic controllers to generate the control torque, τ. In practice, measured wheel velocities, $\dot{\theta}_R$ and $\dot{\theta}_L$, contain noise, which could affect the control performance. Therefore, SMO and HGO are designed to estimate the wheel velocities, $\dot{\hat{\theta}}_R$ and $\dot{\hat{\theta}}_L$. Then, output feedback PD and SMC schemes are designed by integrating the observers into state feedback PD and SMC schemes. CG and load changes are considered as known to apply state feedback and output feedback control techniques. Lastly, the mass of support frame with human, and CG shift are assumed to be unknown, and parameter identifier is integrated to estimate these values. A suitable parametric model is defined, estimation error and estimation model is obtained, a least-square control law is implemented based on this models. Adaptive PD and SMC schemes are designed utilizing the estimated states and parameters.

Chapter 3

State Feedback Control

In this chapter, a state feedback control is designed to provide the path tracking with a given desired position. In order to do so, the control problem is discussed in two parts. First, a kinematic controller based on backstepping approach is designed to obtain the wheel velocities. Then, computed-torque based feedback linearization is applied to have a better solution in path tracking. PD control and SMC techniques are implemented to the feedback linearized system, respectively. The overall system block diagram is illustrated in Fig. 3.1.

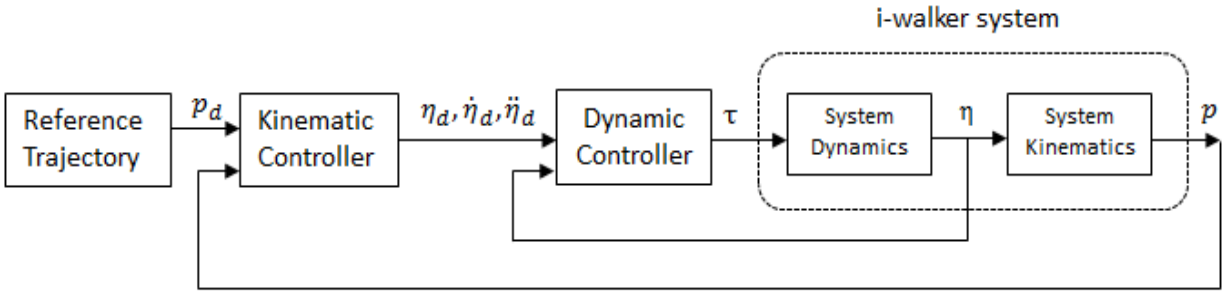

Figure 3.1: Block diagram of overall system.

3.1 Formal Control Problem Definition

Consider the system which is modelled by (2.10). The control objective is to generate appropriate torques, τ_R and τ_L, to have $p(t) = \begin{bmatrix} x(t) & y(t) & \alpha(t) \end{bmatrix}^T$ track a desired trajectory, $p_d(t) = \begin{bmatrix} x_d(t) & y_d(t) & \alpha_d(t) \end{bmatrix}^T$ to ensure $\lim_{t\to\infty}(p_d(t) - p(t)) = 0$. To deal with this problem, we follow a two-level control design approach. At the higher level, a backstepping based kinematic controller is designed to produce the specified velocity vector, $z_d = \begin{bmatrix} v_d & \omega_d \end{bmatrix}^T$, using the kinematic relation in (2.2). At the lower level, a feedback linearization based dynamic controller is designed to generate the control torques τ_R and τ_L required to have v and ω track v_d and ω_d, respectively. One PD control scheme and one SMC are designed for the lower level control task.

3.2 Backstepping Based Kinematic Control Design

In this section, a kinematic controller based on backstepping approach [34] is designed to achieve 'perfect velocity tracking'. The position tracking error $\tilde{p} = p_d - p$ can be expressed in the body fixed coordinate frame as

$$\tilde{p}_b = \begin{bmatrix} e_x & e_y & e_\alpha \end{bmatrix}^T = H\tilde{p}, \tag{3.1}$$

$$H = \begin{bmatrix} cos\alpha & sin\alpha & 0 \\ -sin\alpha & cos\alpha & 0 \\ 0 & 0 & 1 \end{bmatrix}.$$

The derivative of the position tracking error given in (3.1) can be written as follows:

$$\dot{\tilde{p}}_b = \begin{bmatrix} \dot{e}_x \\ \dot{e}_y \\ \dot{e}_\alpha \end{bmatrix} = \begin{bmatrix} \omega e_y - v + \bar{v}_d \cos e_\alpha \\ -\omega e_x + \bar{v}_d \sin e_\alpha \\ \bar{\omega}_d - \omega \end{bmatrix}, \tag{3.2}$$

where $\bar{v}_d = \sqrt{\dot{x}_d^2 + \dot{y}_d^2}$ and $\bar{\omega}_d = \dot{\alpha}_d$. The kinematic controller based on backstepping approach can be designed to produce the 'perfect velocity' control command as follows [35]:

$$z_d = \begin{bmatrix} v_d \\ \omega_d \end{bmatrix} = \begin{bmatrix} \bar{v}_d \cos e_\alpha + K_x e_x \\ \bar{\omega}_d + \bar{v}_d (K_y e_y + K_\alpha \sin e_\alpha) \end{bmatrix}, \tag{3.3}$$

where K_x, K_y, and K_α are positive proportional gains. Later in Section 3.3, dynamic controllers will be designed for $z_A = [v, \omega]^T$ to track z_d in (3.3).

In order to prove the stability of the designed kinematic controller, i.e for the ideal case $z_A = z_d$, the following Lyapunov candidate function is considered:

$$V = \frac{1}{2}\left(e_x^2 + e_y^2\right) + \frac{1 - \cos e_\alpha}{K_y} \tag{3.4}$$

As can be seen from (3.4), $V(\tilde{p}_b)$ is a positive definite function. The derivative of V is obtained as

$$\dot{V} = \dot{e}_x e_x + \dot{e}_y e_y + \frac{\sin e_\alpha}{K_y} \dot{e}_\alpha. \tag{3.5}$$

The following equation can be obtained by substituting (3.2) in (3.5).

$$\begin{aligned} \dot{V} &= \left(\omega_d e_y - v_d + \bar{v}_d \cos e_\alpha\right) e_x + \left(\bar{v}_d \sin e_\alpha - \omega_d e_x\right) e_y - \frac{\sin e_\alpha}{K_y} \left(\bar{\omega}_d - \omega_d\right) \\ &- v_d e_x + \bar{v}_d (e_x \cos e_\alpha + e_y \sin e_\alpha) + \frac{\sin e_\alpha}{K_y} (\bar{\omega}_d - \omega_d) \\ &= -K_x e_x^2 - \frac{K_\alpha \bar{v}_d \sin^2 e_\alpha}{K_y}. \end{aligned} \tag{3.6}$$

As the velocity $\bar{v}_d \geq 0$, the $\dot{V} \leq 0$. Hence, it can be said that $e_x, e_\alpha \to 0$ as $t \to \infty$

3.3 Low Level Dynamic Control Design

In this section, low level dynamic controllers are designed to produce the control torques τ_R and τ_L for $p(t)$ to track a desired trajectory $p_d(t)$. Firstly, computed-torque based feedback linearization is used in the dynamic controller design. The feedback linearized system is integrated with two different types of dynamic control schemes: PD control scheme and SMC scheme.

3.3.1 Feedback Linearization of the System Dynamics

In this section, feedback linearization technique is implemented to have an efficient solution for path tracking based on computed torque control [37]. The aim of feedback linearization in our case is to transform the nonlinear system (2.10), noting state dependence of $\bar{C}$, into an equivalent form linear system to apply linear control techniques [38].

Once an exact dynamic model is known, the control problem becomes easy to solve with the help of computed-torque method. For the system dynamics in (2.10), the state vector and the desired trajectory are $\eta = [\theta_R \quad \theta_L]^T$, $\eta_d = [\theta_{Rd} \quad \theta_{Ld}]^T$, respectively.

In order to ensure the trajectory tracking, a tracking error is defined as follows:

$$e = \eta_d - \eta. \tag{3.7}$$

Through the tracking error e, first and second derivatives are obtained:

$$\begin{aligned} \dot{e} &= \dot{\eta}_d - \dot{\eta}, \\ \ddot{e} &= \ddot{\eta}_d - \ddot{\eta}. \end{aligned} \tag{3.8}$$

Substituting (3.8) in (2.10), we have

$$\ddot{e} = \ddot{\eta}_d + \bar{M}^{-1}(\bar{C}\dot{\eta} - \tau). \tag{3.9}$$

The control input function is defined as

$$u = \ddot{\eta}_d + \bar{M}^{-1}(\bar{C}\dot{\eta} - \tau). \tag{3.10}$$

Defining the states

$$\begin{aligned} X = \begin{bmatrix} X_1 \\ X_2 \end{bmatrix} = \begin{bmatrix} \eta \\ \dot{\eta} \end{bmatrix}, \quad X_d = \begin{bmatrix} \eta_d \\ \dot{\eta}_d \end{bmatrix}, \\ E = \begin{bmatrix} e \\ \dot{e} \end{bmatrix} = X_d - X. \end{aligned} \tag{3.11}$$

the tracking error dynamics (linear error system) are written as

$$\dot{E} = \begin{bmatrix} 0 & I \\ 0 & 0 \end{bmatrix} E + \begin{bmatrix} 0 \\ I \end{bmatrix} u, \tag{3.12}$$

Using (3.10), the computed torque can be written as

$$\tau = \bar{M}(\ddot{\eta}_d - u) + \bar{C}\dot{\eta}. \tag{3.13}$$

3.3.2 Proportional-Derivative Control Design

The auxiliary control signal, $u(t)$, can be chosen by using various control approaches, including robust and adaptive ones. In this section, we perform a PD control design:

$$u = -K_d\dot{e} - K_p e = -\begin{bmatrix} K_p & K_d \end{bmatrix} E, \tag{3.14}$$

where $K_p, K_d \in \mathbb{R}^{2x2}$ are diagonal block P and D control gains, respectively. Substituting (3.14) in (3.13), the *computed torque control law* can be obtained

$$\tau = \bar{M}(\ddot{\eta}_d + K_d\dot{e} + K_p e) + \bar{C}\dot{\eta}. \tag{3.15}$$

This controller is shown in Fig. 3.2. Substituting (3.14) in (3.12), closed-loop error dynamics in the state space form becomes

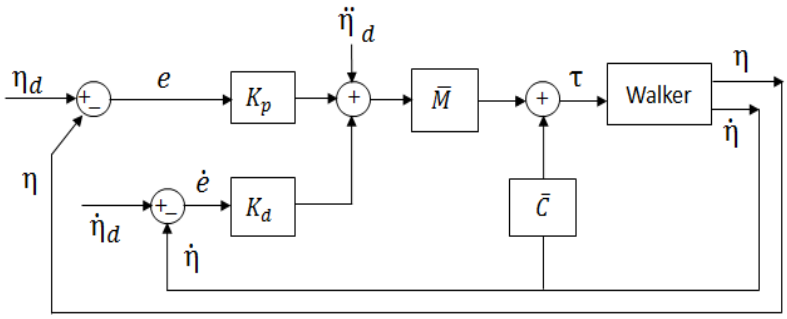

Figure 3.2: PD controller.

$$\dot{E} = A_{pd}E, \tag{3.16}$$

where $A_{pd} = \begin{bmatrix} 0 & I \\ -K_p & -K_d \end{bmatrix}$.

In order to establish the stability of proposed controller, let us examine the eigenvalues of A_{pd} based on the stability approach in [39]. We aim to show that each eigenvalue of A_{pd} has negative real part. Let $\lambda \in \mathbb{C}$ be an eigenvalue of A_{pd} with the corresponding eigenvector $\vartheta = \left[\vartheta_1^T, \vartheta_2^T\right]^T \in \mathbb{C}^4$, $\vartheta \neq 0$.

$$\lambda \begin{bmatrix} \vartheta_1 \\ \vartheta_2 \end{bmatrix} = A_{pd} \begin{bmatrix} \vartheta_1 \\ \vartheta_2 \end{bmatrix} = \begin{bmatrix} 0 & I \\ -K_p & -K_d \end{bmatrix} \begin{bmatrix} \vartheta_1 \\ \vartheta_2 \end{bmatrix} = \begin{bmatrix} \vartheta_2 \\ -K_p\vartheta_1 - K_d\vartheta_2 \end{bmatrix} \tag{3.17}$$

Assuming $\| \vartheta_1 \| = 1$, we can write the following equation.

$$\begin{aligned} \lambda^2 = \vartheta_1^* \lambda \vartheta_2 = \vartheta_1^* \left(-K_p\vartheta_1 - K_d\vartheta_2\right) &= -\vartheta_1^* K_p \vartheta_1 - \vartheta_1^* K_d \vartheta_2 \\ &= -\vartheta_1^* K_p \vartheta_1 - \lambda \vartheta_1^* K_d \vartheta_1, \end{aligned} \tag{3.18}$$

where ϑ_1^* represents the complex conjugate transpose of ϑ_1. Then, we obtain

$$\lambda^2 + a\lambda + b = 0, \tag{3.19}$$

where $a = \vartheta_1^* K_d \vartheta_1 > 0$, and $b = \vartheta_1^* K_p \vartheta_1 > 0$. From (3.19), we can see that the real part of eigenvalue, λ, is negative.

3.3.3 Sliding Mode Control Design

Sliding mode control (SMC) is an efficient control method to design robust controllers since it helps reduce the complexity of feedback design; and has applications in a variety of areas, including robotics, vehicles, and power systems [38].
Considering the state definition in (3.11), (2.10) can be written in the form

$$\begin{aligned} \dot{X}_1 &= X_2, \\ \dot{X}_2 &= -\bar{M}^{-1}(X)\,\bar{C}(X)\,X_2 + \bar{M}^{-1}(X)\,\tau. \end{aligned} \tag{3.20}$$

Control objective is to bring state X to the desired state X_d. In order to do so, tracking error is considered as in (3.11). Sliding surface is related to the tracking error and its derivative. It provides the tracking error goes to zero in finite time. A time varying sliding surface can be defined by the constraint

$$s(E,t) = 0, \tag{3.21}$$

where

$$s(E,t) = \dot{e}(t) + \lambda e(t), \quad \lambda > 0, \tag{3.22}$$

λ is a strictly positive constant. The SMC design will aim moving $s(E,t)$ to (3.21) and keeping it there. For this purpose, consider the Lyapunov function

$$V_s(s) = \frac{s^T s}{2}. \tag{3.23}$$

The SMC is designed to satisfy

$$\dot{V}_s = s^T \dot{s} = -k_1 \parallel s \parallel, \tag{3.24}$$

for some design coefficient $k_1 > 0$. This condition will guarantee that the sliding surface is reached in finite time [38]. (3.23) can be satisfied by selecting to control law so that the derivative of s satisfies

$$\dot{s} = -k_1 sgn(s), \tag{3.25}$$

where

$$sgn(s) = sgn\left(\left[s_1, s_2\right]^T\right) = \left[sgn(s_1), sgn(s_2)\right]^T, \tag{3.26}$$

Now we design the control input τ to satisfy (3.25). First, τ_0 can be chosen as

$$\tau_0 = -\bar{M}(X)\left(-\bar{M}^{-1}(X)\,\bar{C}(X)\,X_2 - \ddot{\eta}_d - \lambda\dot{e}\right). \tag{3.27}$$

Then the overall control input τ can be selected as

$$\tau = \tau_0 - \bar{M}(X)k_1 sgn(s), \tag{3.28}$$

so that (3.20) and (3.28) together result in (3.25). In use of the control law (3.28), chattering problems occur because of the discontinuity of sgn function. To deal with such chattering problems, $k_1 sgn(s)$ term is replaced with $k_1 sat(s/\bar{\epsilon})$:

$$sat(s/\bar{\epsilon}) = \begin{cases} -1, & s < -\bar{\epsilon} \\ s/\bar{\epsilon}, & -\bar{\epsilon} < s < \bar{\epsilon} \\ 1, & s > \bar{\epsilon} \end{cases} \tag{3.29}$$

where $\bar{\epsilon}$ is a design parameter (boundary layer thickness).

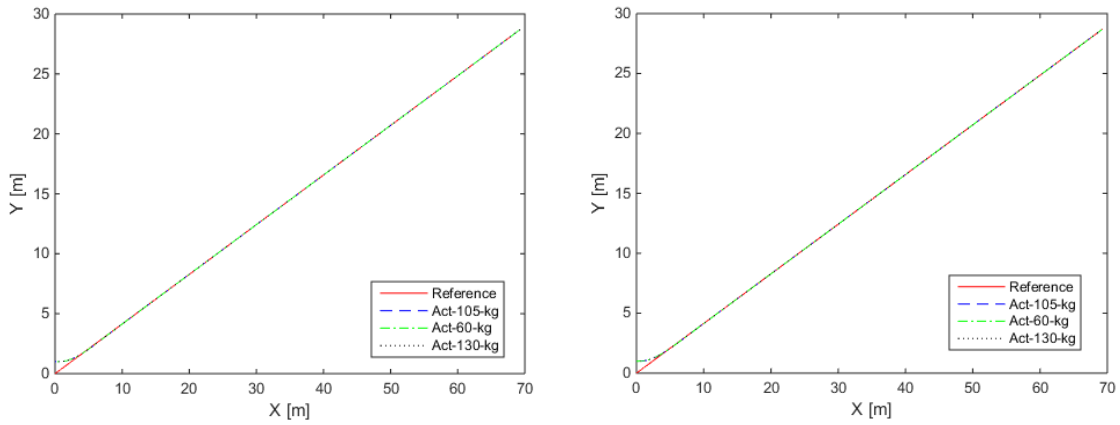

Figure 3.3: Straight line tracking results for (a) PD controller and (b) SMC.

3.4 Simulations

In this section, simulation results are presented in order to verify the validity of the proposed state feedback controllers for path tracking. Two different motion characteristics, straight and curved, are tested to be tracked by the point A on the i-walker system for both PD controller and SMC. First, straight line trajectory tracking is examined. Then, "8" figure trajectory tracking results are discussed as a sample curved motion.

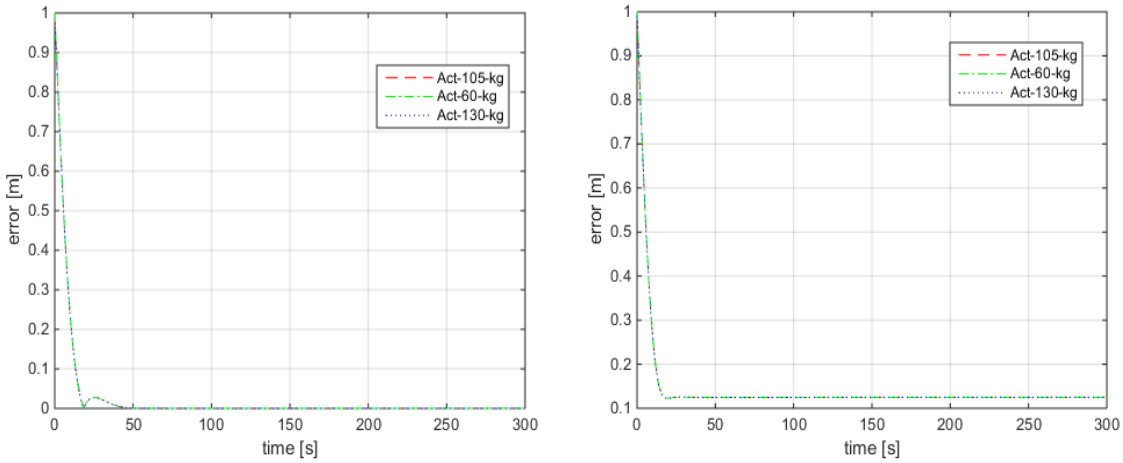

(a) (b)

Figure 3.4: Straight line tracking errors for (a) PD controller and (b) SMC.

The physical parameters of the i-walker in the simulation are selected as $r = 0.15m$, $b_m = 0.4kg.m^2/s$, $I_c = 5.04kg.m^2$, $I_w = 0.0144kg.m^2$, $I_m = 0.0125kg.m^2$, $m_c = (26, 36, 46)kg$, $m_w = 1kg$, $d = (0.18, 0.1125, 0.0818)m$. $K_x = 0.4$, $K_y = 0.4$, $K_\alpha = 1$ are chosen. A certain percentage of m can be applied to the i-walker system. We assume that the user mass ranges from 60 kg to 130 kg. Thus, the upper limit is determined based on the assumption that the user having 130 kg mass applied the force on handles as much as 20% of the user body weight. The lower limit is considered that the user with 60 kg mass applies the force to the handles 10% of the user body weight [40]. The saturation bounds for τ_R and τ_L are set as $\mp 3N.m$. $K_p = 8.5$, $K_d = 4$ used in the PD control algorithm are positive design parameters. $\lambda = 15$, $k_1 = 5$, and $\bar{\epsilon} = 0.01$ constants are given for SMC. We considered two

cases that are straight and 8 figure.

Case 1: The desired path for the straight trajectory is defined as

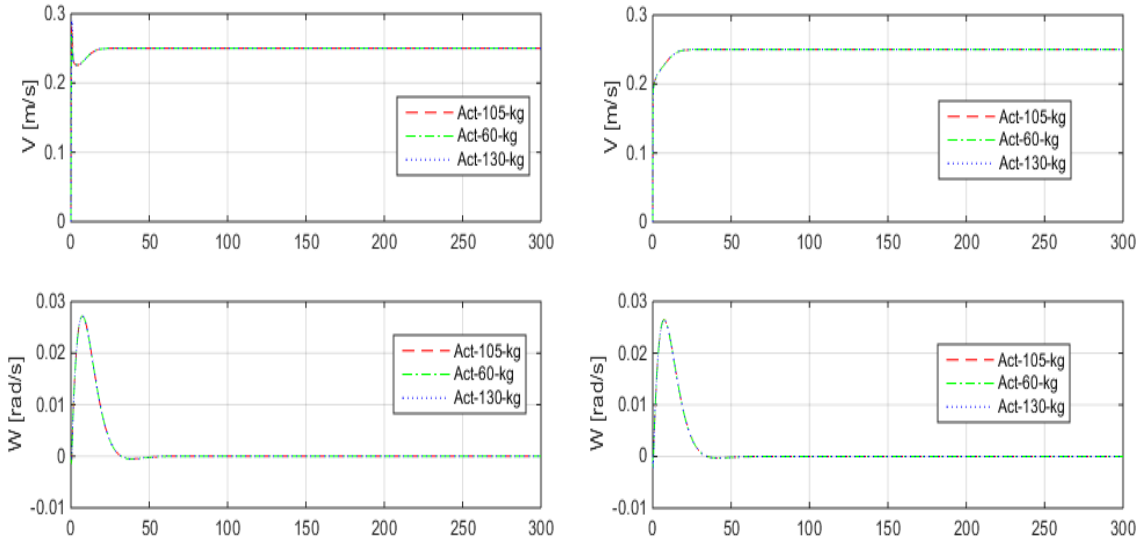

(a) (b)

Figure 3.5: Straight line velocities for (a) PD controller and (b) SMC.

$$\begin{aligned} x_d &= tv_d \cos(\alpha), \\ y_d &= tv_d \sin(\alpha), \end{aligned} \tag{3.30}$$

and the derivative of the trajectory is given as

$$\begin{aligned} \dot{x}_d &= v_d \cos(\alpha), \\ \dot{y}_d &= v_d \sin(\alpha) \end{aligned} \tag{3.31}$$

The straight path is defined as $x_d = 0.25t\cos\left(\frac{\pi}{8}\right)$, $y_d = 0.25t\sin\left(\frac{\pi}{8}\right)$, $\alpha_d = \pi/8$ and the initial conditions are given as $(x_0, y_0, \alpha_0) = (0, 1, 0)$.

Case 2: For the figure eight path tracking, the desired path is defined as

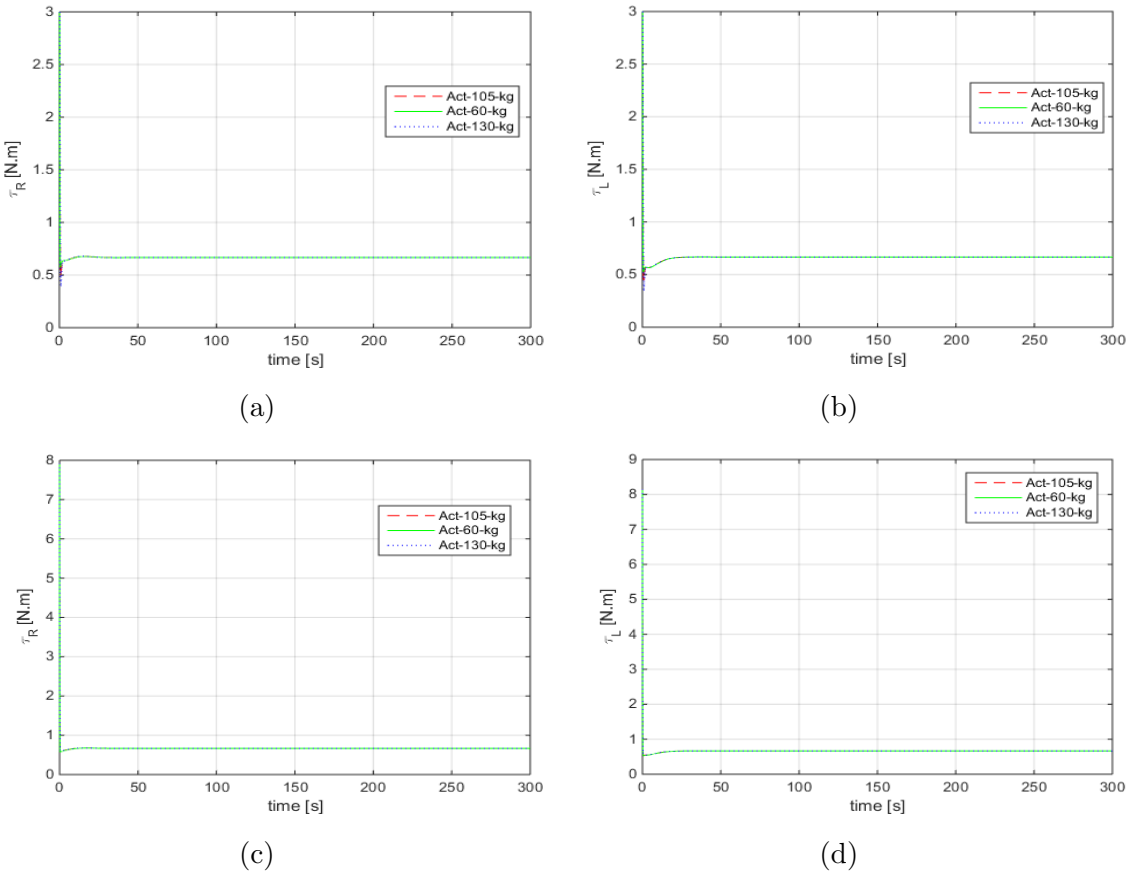

Figure 3.6: Straight line control torques of right and left wheels for (a,b) PD controller and (c,d) SMC.

$$\begin{aligned} x_d &= R\sin(2\omega t) \quad y_d = R\cos(\omega t) - R \\ \dot{x}_d &= 2R\omega\cos(2\omega t) \quad \dot{y}_d = -R\omega\sin(\omega t) \end{aligned} \tag{3.32}$$

In order to feed the trajectory into a controller, the heading angle and forward velocity are also defined as

$$v_d = \sqrt{\dot{x}_d^2 + \dot{y}_d^2} \quad \alpha_d = atan2(\dot{y}_d, \dot{x}_d) \tag{3.33}$$

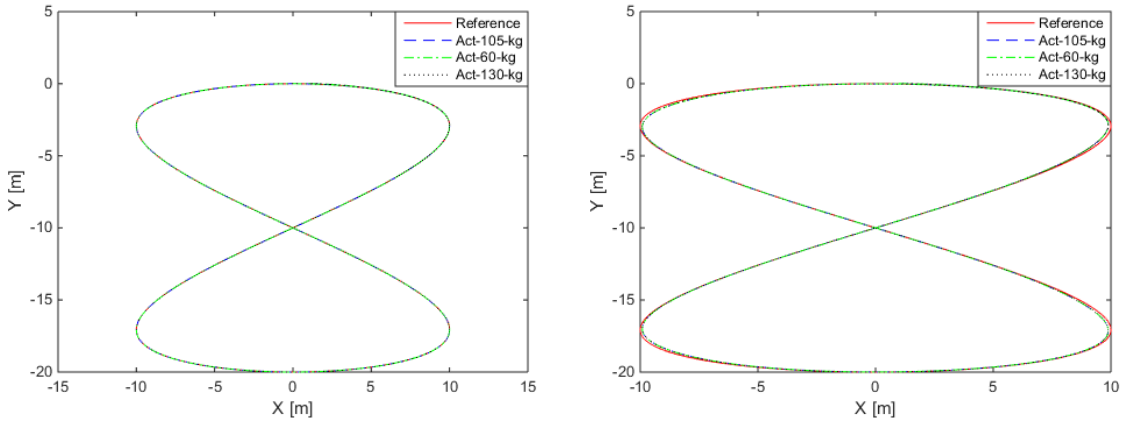

(a) (b)

Figure 3.7: Figure eight tracking results for (a) PD controller and (b) SMC.

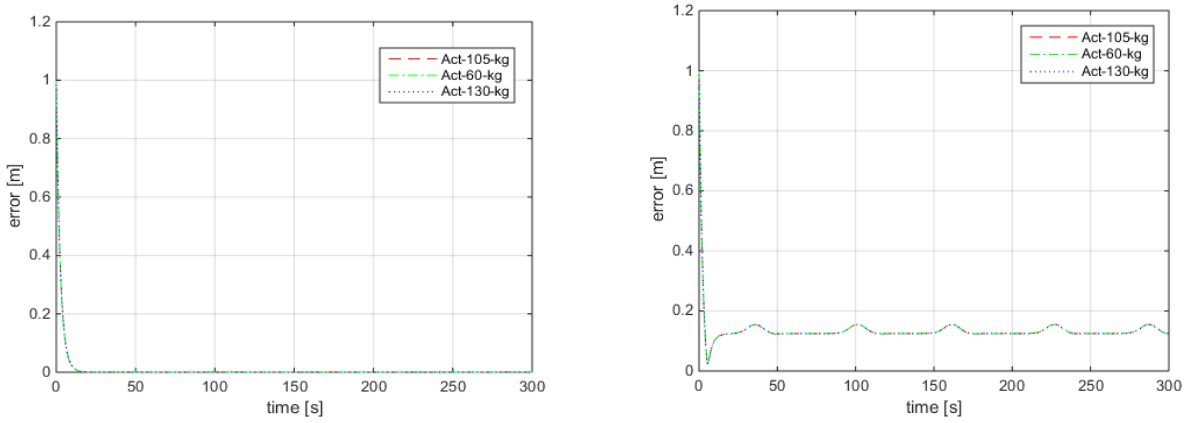

(a) (b)

Figure 3.8: Figure eight tracking errors for (a) PD controller and (b) SMC.

The figure eight trajectory is defined as $x_d = 10sin(0.05t)$ and $y_d = 10cos(0.025t) - 10$. The initial conditions for figure eight are chosen as $(x_0, y_0, \alpha_0) = (1, 0.01, 0)$.

Simulation results for the straight line trajectory are plotted in Figs. 3.3-3.6. Fig. 3.3 presents the tracking results in (x,y) plane, Fig. 3.4 displays the tracking errors, Figs. 3.5

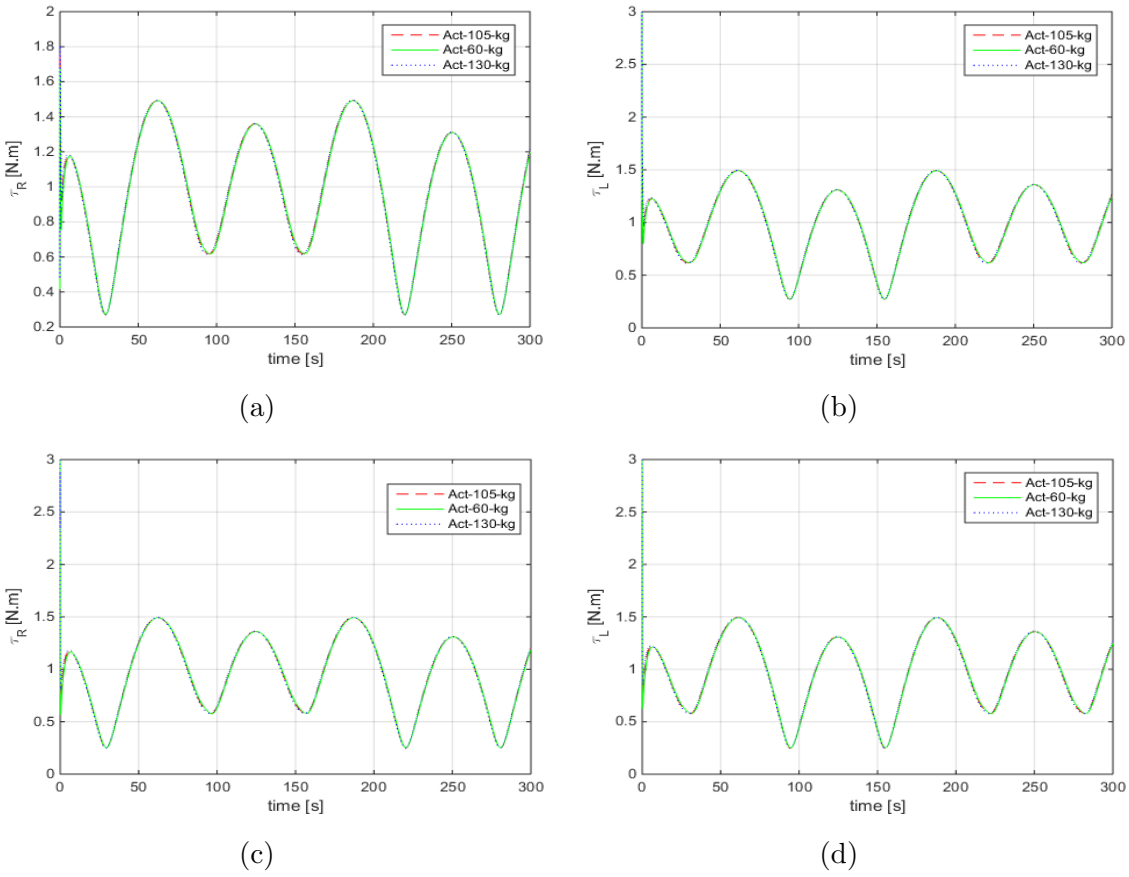

Figure 3.9: Figure eight control torques of right and left wheels for (a,b) PD controller and (c,d) SMC.

shows the velocities, Fig. 3.6 plots the control torques for both PD control and SMC.

Similar to straight line, figure eight simulations are given in Figs. 3.7-3.10. Fig. 3.7 shows the tracking results, Fig. 3.8 displays the tracking errors, Figs. 3.9 presents the control torques, Fig. 3.10 plots the velocities for both PD control and SMC.

As can be seen from the figures that the i-walker system is following the desired trajectory, tracking errors converge to zero in time. The proposed control schemes, PD control and SMC, are effective for path tracking, as verified by simulations.

Additionally, due to the chattering issues, saturation function is introduced to SMC.

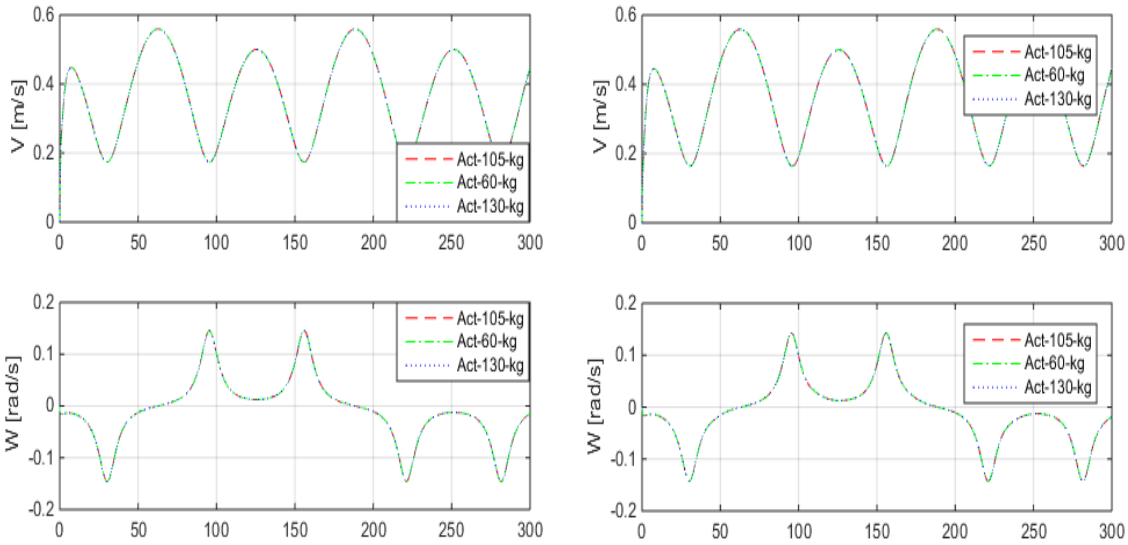

(a) (b)

Figure 3.10: Figure eight velocities for (a) PD controller and (b) SMC.

Therefore, the steady-state error in SMC results has not reached to zero.

Chapter 4

Observer Design and Output Feedback Control

In Chapter 3, state feedback controllers have been developed to track desired trajectories for i-walkers. In practice, the positions of i-walkers can be accurately measured using encoders. Velocity is also measured by some devices like tachometers. However, velocity measurements mostly carry noise, which may affect the performance of the motion control system. For this reason, it is necessary to integrate an estimator to the control scheme for obtaining reliable velocity information.

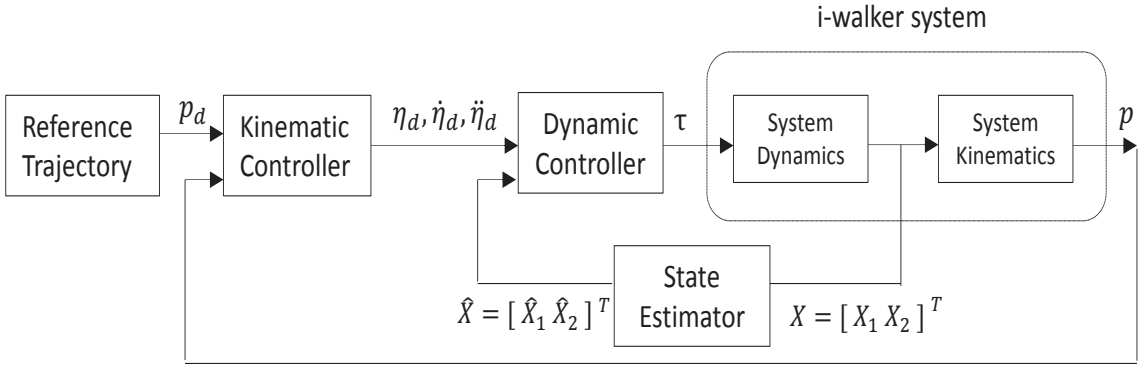

Figure 4.1: Block diagram of output feedback control with state estimation.

To design the estimator using the state definition in (3.11), the state-space system representation (3.20) is considered. Main objective of the estimator design is to produce a state estimate $\hat{X} = [\hat{X}_1^T \quad \hat{X}_2^T]^T = [\hat{\eta}^T \quad \dot{\hat{\eta}}^T]^T$ that asymptotically tracks the actual state $X = [X_1^T \quad X_2^T]^T = [\eta^T \quad \dot{\eta}^T]^T$, i.e. $\tilde{X}(t) = \hat{X}(t) - X(t) \to 0$ asymptotically as $t \to \infty$. Two kinds of observers, sliding mode observer (SMO) and high gain observer (HGO), are considered to estimate the system state. Later, state-space PD control and SMC schemes of Chapter 3 are integrated with the designed SMO and HGO to form output feedback controllers. Fig. 4.1 represents the block diagram of the closed loop output feedback control system.

4.1 Sliding Mode Observer Design

SMOs have advantages similar to those of SMCs, especially being robust to parameter uncertainties. In addition, chattering issues in SMOs only occur in numerical implementations in contrast to SMCs [22]. To design an SMO, consider the system model given in (3.20). In order to estimate the state X_2, an SMO is designed following the procedure of [22] as

$$\begin{aligned} \dot{\hat{X}}_1 &= -a_1\tilde{X}_1 + \hat{X}_2 - k_1 sgn(\tilde{X}_1), \\ \dot{\hat{X}}_2 &= -a_2\tilde{X}_1 - \bar{M}^{-1}\bar{C}\left(\hat{X}_2\right)\hat{X}_2 + \bar{M}^{-1}\tau - k_2 sgn(\tilde{X}_1), \end{aligned} \tag{4.1}$$

where $y = X_1$, a_1, a_2, k_1, and k_2 are positive gains; $\hat{X}_1$ and $\hat{X}_2$ are the estimates of X_1 and X_2, respectively; $\tilde{X}_1 = \hat{X}_1 - X_1$.

$$\begin{aligned} \dot{\tilde{X}}_1 &= -a_1\tilde{X}_1 + \tilde{X}_2 - k_1 sgn(\tilde{X}_1), \\ \dot{\tilde{X}}_2 &= -a_2\tilde{X}_1 - k_2 sgn(\tilde{X}_1) + \delta(X_2, \hat{X}_2), \\ \delta(X_2, \hat{X}_2) &= \bar{M}^{-1}(\bar{C}(X_2)X_2 - \bar{C}(\hat{X}_2)\hat{X}_2), \end{aligned} \tag{4.2}$$

where a_1 and a_2 are chosen such that the Hurwitz matrix $A_0 = \begin{bmatrix} -a_1 & I \\ -a_2 & 0 \end{bmatrix}$ has the desired set of eigenvalues. Note that, $y = X_1$ is already available for measurement; the purpose of the (non-reduced-order) observer (4.1) is to produce $\hat{X}_2$; and $\hat{X}_1$ is produced only for feeding and stabilizing the observer.

Stability analysis of the SMO design can be performed rewriting (4.2) as

$$\dot{\tilde{X}} = A_0\tilde{X} - K_0 sgn(\tilde{X}_1) + \Delta, \tag{4.3}$$

where $K_0 = \begin{bmatrix} k_1 & I_{2x2} \\ k_2 & I_{2x2} \end{bmatrix}$, $\Delta = \begin{bmatrix} 0_{2x1} \\ \delta(X_2, \hat{X}_2) \end{bmatrix}$. Conditions on a_1, a_2, k_1, k_2, and $\delta(X_2, \hat{X}_2)$ for guaranteeing $\tilde{X}$ to be uniformly ultimately bounded, i.e., to converge to a ball around zero with a pre-set radius, can be found in [22].

4.2 High Gain Observer Design

In this section, an HGO design is considered instead of SMO to estimate the state X_2. The aim of the HGO is to make the system robust to uncertainties [41]. Again, considering the system in (3.20), the following HMO is designed:

$$\begin{aligned} \dot{\hat{X}}_1 &= \hat{X}_2 - l_1\tilde{X}_1, \\ \dot{\hat{X}}_2 &= -l_2\tilde{X}_1 - \bar{M}^{-1}\bar{C}\left(\hat{X}_2\right)\hat{X}_2 + \bar{M}^{-1}\tau, \end{aligned} \tag{4.4}$$

where $l_1 = \frac{a_1}{\epsilon_h}$, $l_2 = \frac{a_2}{\epsilon_h^2}$ for some $0 < \epsilon_h << 1$ and $a_1, a_2 > 0$ are chosen so that the Hurwitz polynomial $s^2 + a_1 s + a_2$ has the desired set of roots. Estimation error equations, considering (3.20), (4.4), can be found as

$$\begin{aligned} \dot{\tilde{X}}_1 &= -l_1\tilde{X}_1 + \tilde{X}_2, \\ \dot{\tilde{X}}_2 &= -l_2\tilde{X}_1 + \delta(X_2, \hat{X}_2). \end{aligned} \tag{4.5}$$

Similar to (4.3), (4.5) can be rewritten as

$$\dot{\tilde{X}} = L_0\tilde{X} + \Delta, \tag{4.6}$$

for

$$L_0 = \begin{bmatrix} -l_1 & 1 \\ -l_2 & 0 \end{bmatrix}. \tag{4.7}$$

It is established in [42] that, (4.6) can be guaranteed to be uniformly ultimately bounded that converges to a ball around zero if ϵ_h is chosen small enough.

4.3 Output Feedback Proportional Derivative Control

To form an output feedback PD control scheme, the state feedback PD control law (3.14) can be integrated with either the SMO (4.1) or the HGO (4.4). Accordingly, the control law (3.14) is replaced with

$$\hat{u} = -\begin{bmatrix} K_p & K_d \end{bmatrix} \hat{E}, \tag{4.8}$$

where $\hat{E} = [\hat{E}_1^T, \hat{E}_2^T]^T = X_d - \hat{X}$. Similarly, the *computed torque control law* (3.13) is redesigned as

$$\tau = \bar{M}(\ddot{\eta}_d - \hat{u}) + \bar{C}(\hat{X}_2)\hat{X}_2. \tag{4.9}$$

The closed loop output feedback PD control system is summarized by (4.1) (or (4.4)), (4.8), (4.9). If we substitute (4.9) in (3.10), we have

$$\begin{aligned} u &= \ddot{\eta}_d + \bar{M}^{-1}\left(\bar{C}(X_2)X_2 - \bar{M}\ddot{\eta}_d + \bar{M}\hat{u} - \bar{C}(\hat{X}_2)\hat{X}_2\right) \\ &= \delta(X_2, \hat{X}_2) + \hat{u}. \end{aligned} \tag{4.10}$$

(4.10) can be rewritten as

$$u = \delta - [K_p K_d]E + [K_p \quad K_d]\tilde{X}, \tag{4.11}$$

then, error dynamics is written as follows:

$$\dot{E} = A_{pd}E + \begin{bmatrix} 0 \\ \delta \end{bmatrix} + \begin{bmatrix} 0 & 0 \\ K_p & K_d \end{bmatrix} \tilde{X}. \tag{4.12}$$

Defining the error state as $[E \quad \tilde{X}]^T$, (4.6) and (4.12) is written as

$$\begin{bmatrix} \dot{E} \\ \dot{\tilde{X}} \end{bmatrix} = \begin{bmatrix} A_{pd} & \begin{bmatrix} 0 & 0 \\ K_p & K_d \end{bmatrix} \\ 0 & L_0 \end{bmatrix} \begin{bmatrix} E \\ \tilde{X} \end{bmatrix} + \begin{bmatrix} \Delta \\ \Delta \end{bmatrix} \tag{4.13}$$

A_{pd} and L_0 are Hurwitz, K_p and K_d are positive constants, and hence stability requirement met.

4.4 Output Feedback Sliding Mode Control

In this section, output feedback SMC is redesigned. Consider the system dynamics (3.20) in state feedback control. We can redesign our SMC scheme (3.27),(3.28), replacing X with $\hat{X}$:

$$\hat{s}(\hat{E},t) = \dot{\hat{E}}_2(t) + \lambda \hat{E}_1(t), \quad \lambda > 0. \tag{4.14}$$

Regarding the sliding conditions in Section 3.3.3, τ_0 can be chosen as follows:

$$\tau_0 = -\bar{M}\left(-\bar{M}^{-1}\bar{C}\left(\hat{X}_2\right)\hat{X}_2 - \ddot{\eta}_d - \lambda\dot{\hat{E}}_2\right), \tag{4.15}$$

$$\tau = \tau_0 - \bar{M}k_1 sgn(\hat{s}), \tag{4.16}$$

For the chattering issues, $k_1 sgn(\hat{s})$ term is replaced with $k_1 sat(\hat{s}/\bar{\epsilon})$ as done in (3.29). Control objective is still to bring the $\hat{X}$ to the desired state X_d, i.e. to have the tracking error $E = X_d - X$ decay to zero. Establishment of the asymptotic tracking in output feedback control case relies on having the observer to satisfy convergence of $\tilde{X} = \hat{X} - X$ to zero (or a small pre-defined ball around zero) and having the controller to guarantee convergence of $\hat{E} = X_d - \hat{X}$ to zero. A detailed stability and convergence analysis can be performed following the procedures in [22, 42].

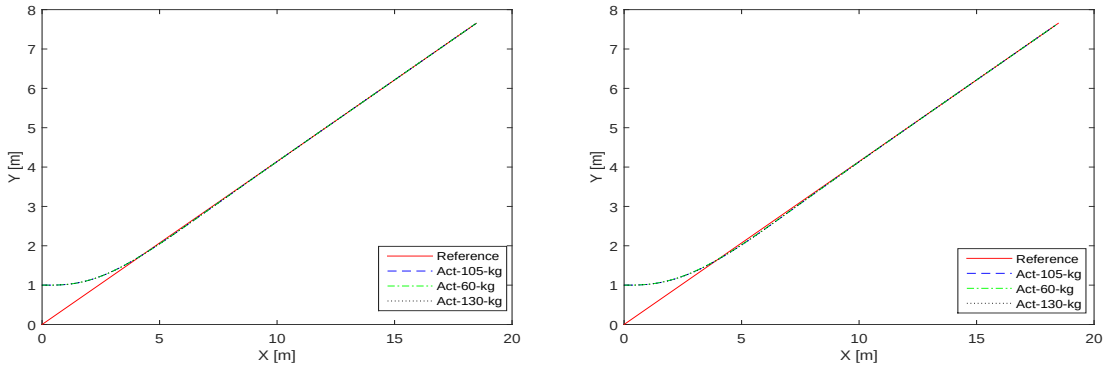

(a) (b)

Figure 4.2: Straight line tracking results for (a) PD controller and (b) SMC with SMO.

4.5 Simulations

In this section, simulation results are presented to see the tracking performance with observers. The physical parameters of the i-walker system are given the same as in Chapter 3. For the SMO, $a_1 = 3.8$, $a_2 = 7.2$, $k_1 = 0.1$, and $k_2 = 2$ are given to the system. $\epsilon_h = 1$, $L_1 = 2$ and $L_2 = 3$ gains are considered for HGO. Also, a constant noise $n = 0.02$ are added to the system.

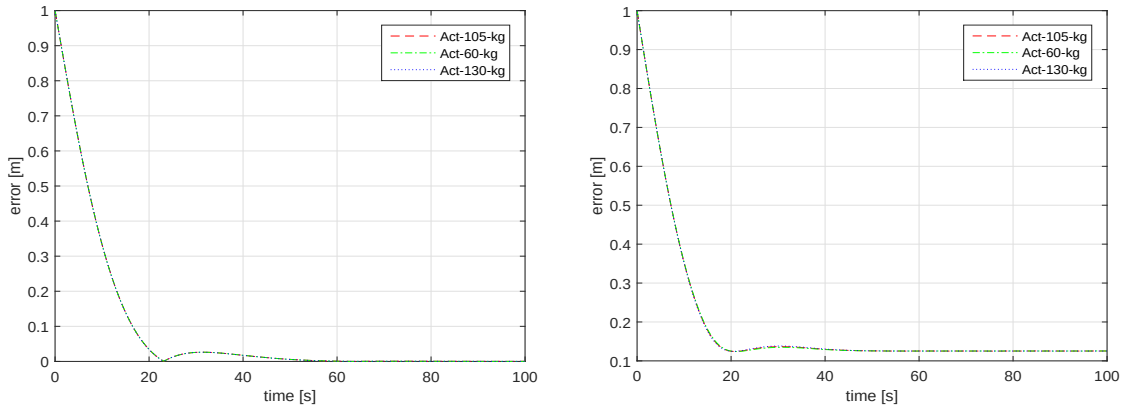

(a) (b)

Figure 4.3: Straight line tracking errors for (a) PD controller and (b) SMC with SMO.

Case 1: The straight path is defined as $x_d = 0.25t\cos\left(\frac{\pi}{8}\right)$, $y_d = 0.25t\sin\left(\frac{\pi}{8}\right)$, $\alpha_d = \pi/8$ and the initial conditions are given the same as in Chapter 3. Trajectory tracking results are given both SMO and HGO.

Simulation results for the straight line trajectory are plotted for SMO in Figs. 4.2-4.5, for HGO in Figs. 4.12-4.15. Figs. 4.2 and 4.12 present the tracking results in (x,y) plane, Figs. 4.3 and 4.13 display the tracking errors, Figs. 4.4 and 4.14 show the velocities, Figs. 4.5 and 4.15 plots the control torques for both PD control and SMC.

Case 2: The figure eight trajectory is defined as $x_d = 10sin(0.05t)$ and $y_d = 10cos(0.025t) - 10$. The initial conditions for figure eight are chosen as $(x_0, y_0, \alpha_0) = (0, 1, \pi/8)$.

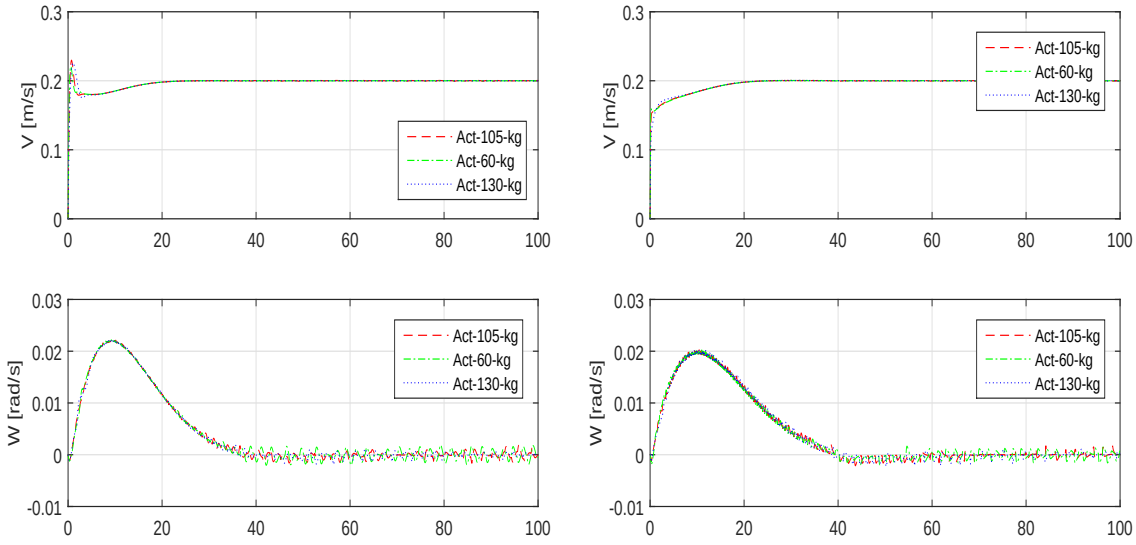

(a) (b)

Figure 4.4: Straight line velocities for (a) PD controller and (b) SMC with SMO.

Similar to straight line, figure eight simulations are given for SMO in Figs 4.6-4.9, for HGO in Figs. 4.16-4.19. Figs. 4.6 and 4.16 show the tracking results, Fig. 4.7 and 4.17 display the tracking errors, Figs. 4.8 and 4.18 present the control torques, Fig. 4.9 and 4.19 plot the velocities for both PD control and SMC.

The simulation results demonstrate that the i-walker system is following the desired trajectory with estimated states, tracking errors converge to zero. The proposed control schemes, PD and SMC, and observers, SMO and HGO, are effective for path tracking, since in each scheme i-walker system tracking task is well achieved.

4.10, 4.11, 4.20, 4.21 demonstrate the results of state estimation for SMO and HGO. As can be seen from the figures that estimated states converge to the actual states, $\hat{X} \rightarrow X$. Therefore, proposed observers and controllers are applicable to make the system robust to CG shifts and load changes for different loads.

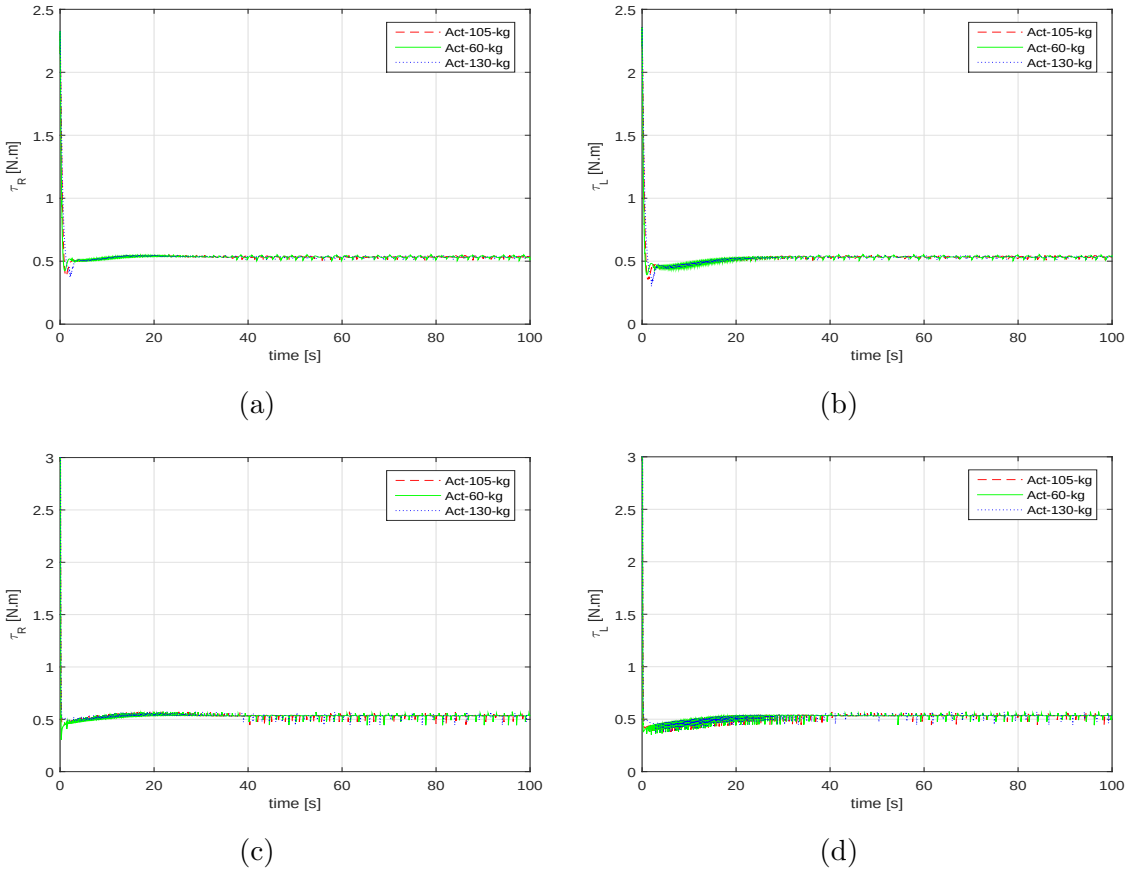

Figure 4.5: Straight line control torques of right and left wheels for (a) PD controller and (b) SMC with SMO.

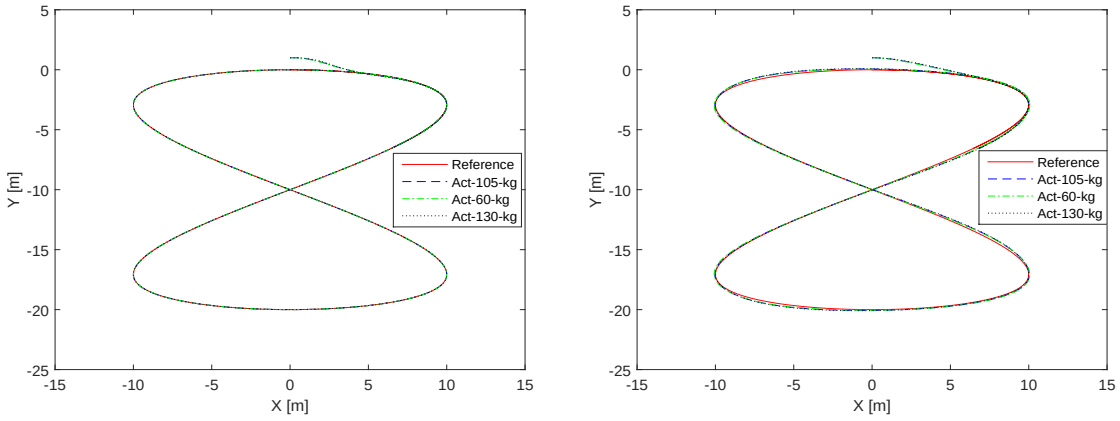

(a) (b)

Figure 4.6: Figure eight tracking results for (a) PD controller and (b) SMC with SMO.

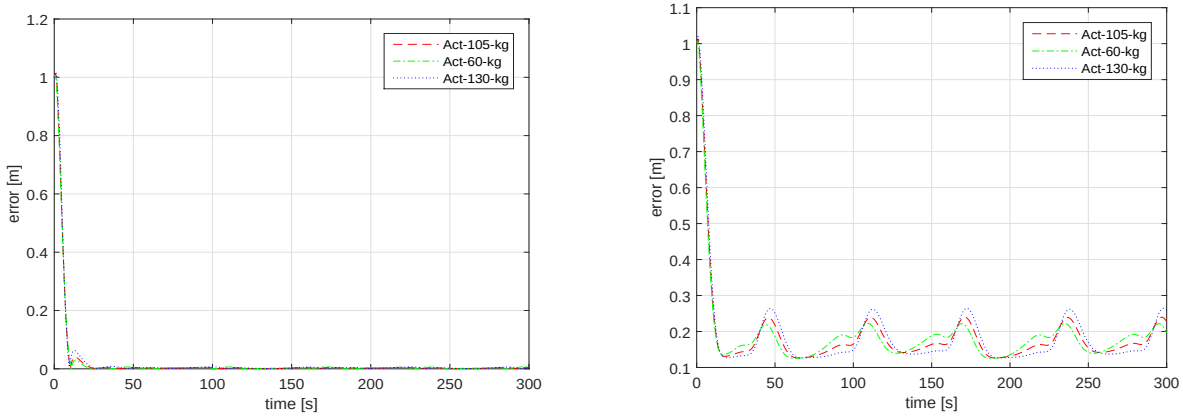

(a) (b)

Figure 4.7: Figure eight tracking errors for (a) PD controller and (b) SMC with SMO.

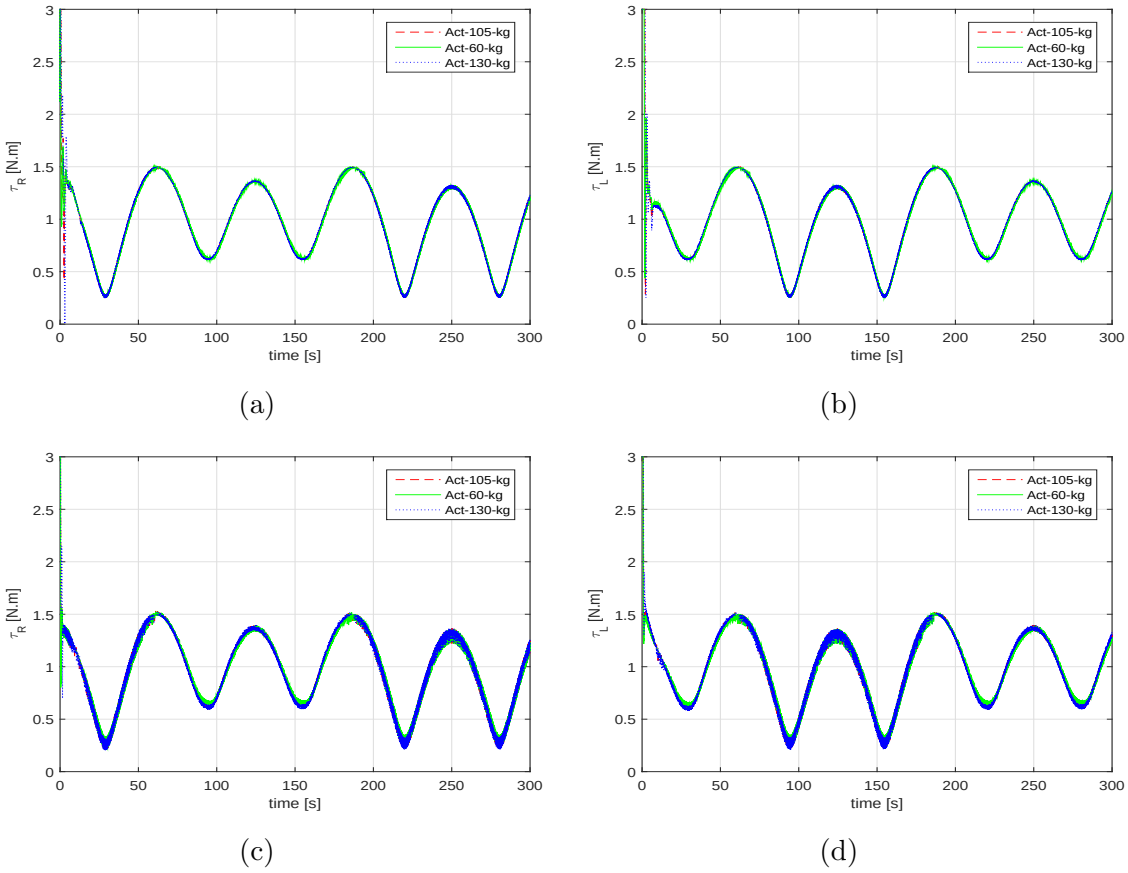

Figure 4.8: Figure eight control torques of right and left wheels for (a,b) PD controller and (c,d) SMC with SMO.

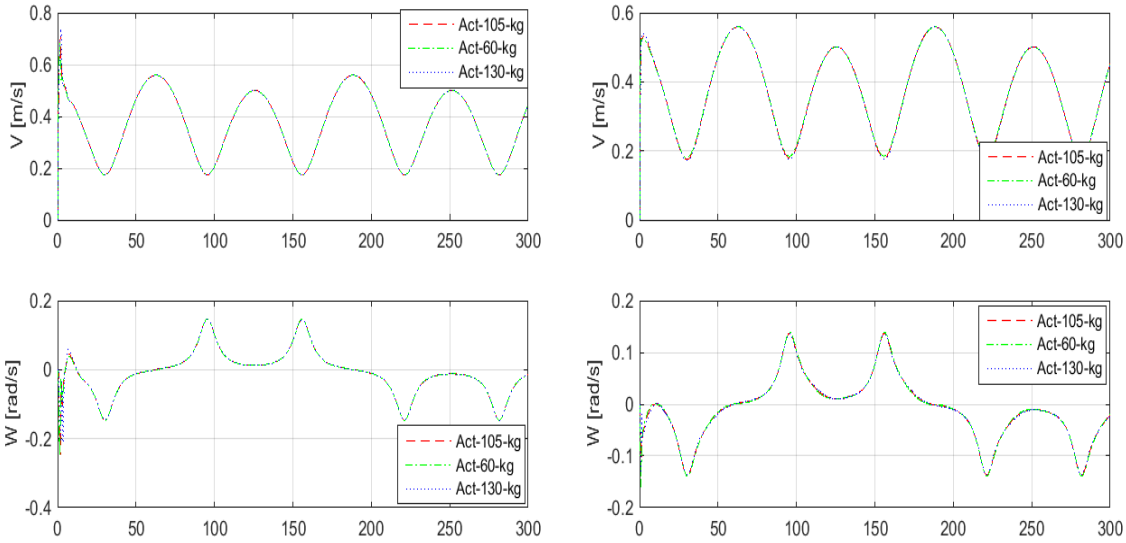

Figure 4.9: Figure eight velocities for (a) PD controller and (b) SMC with SMO.

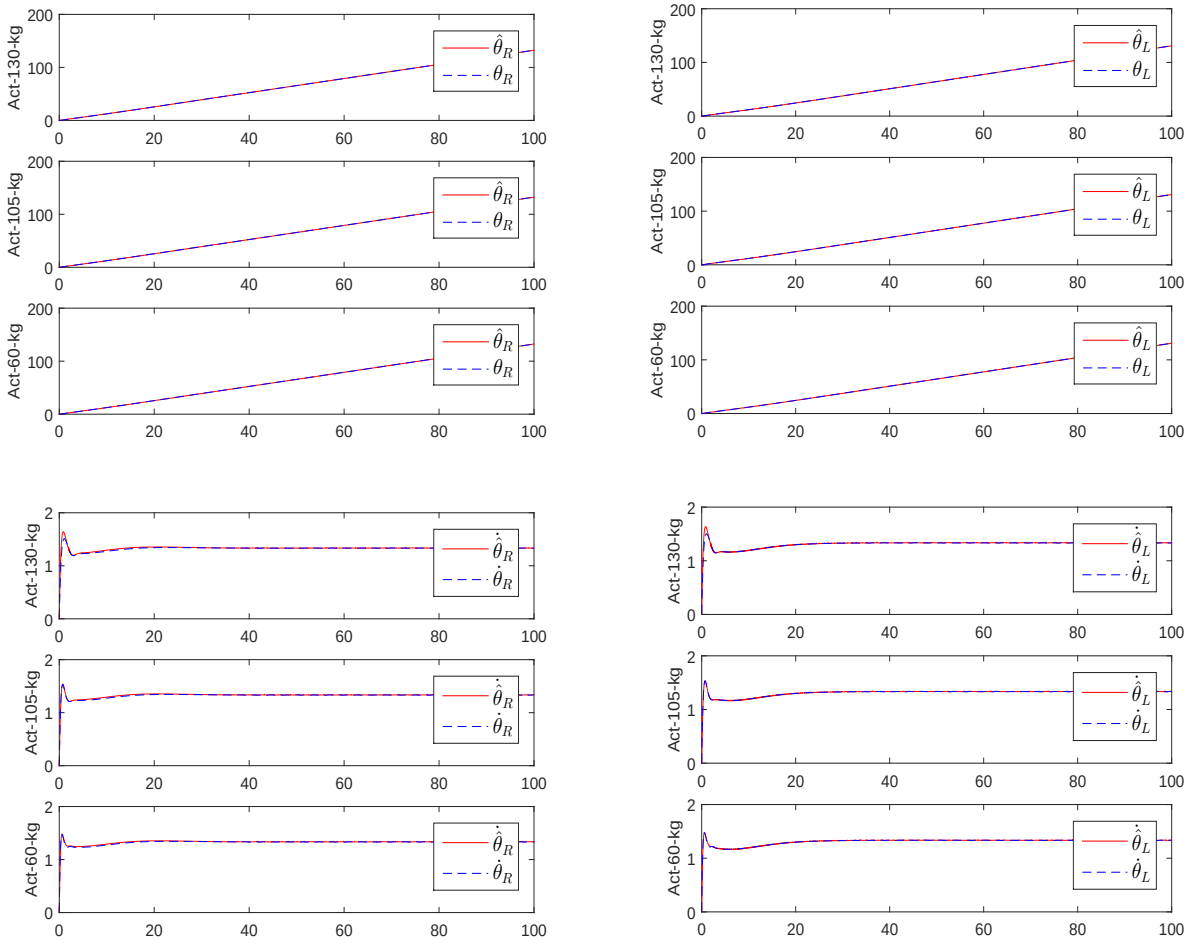

Figure 4.10: Straight line SMO estimation results for wheel positions and velocities.

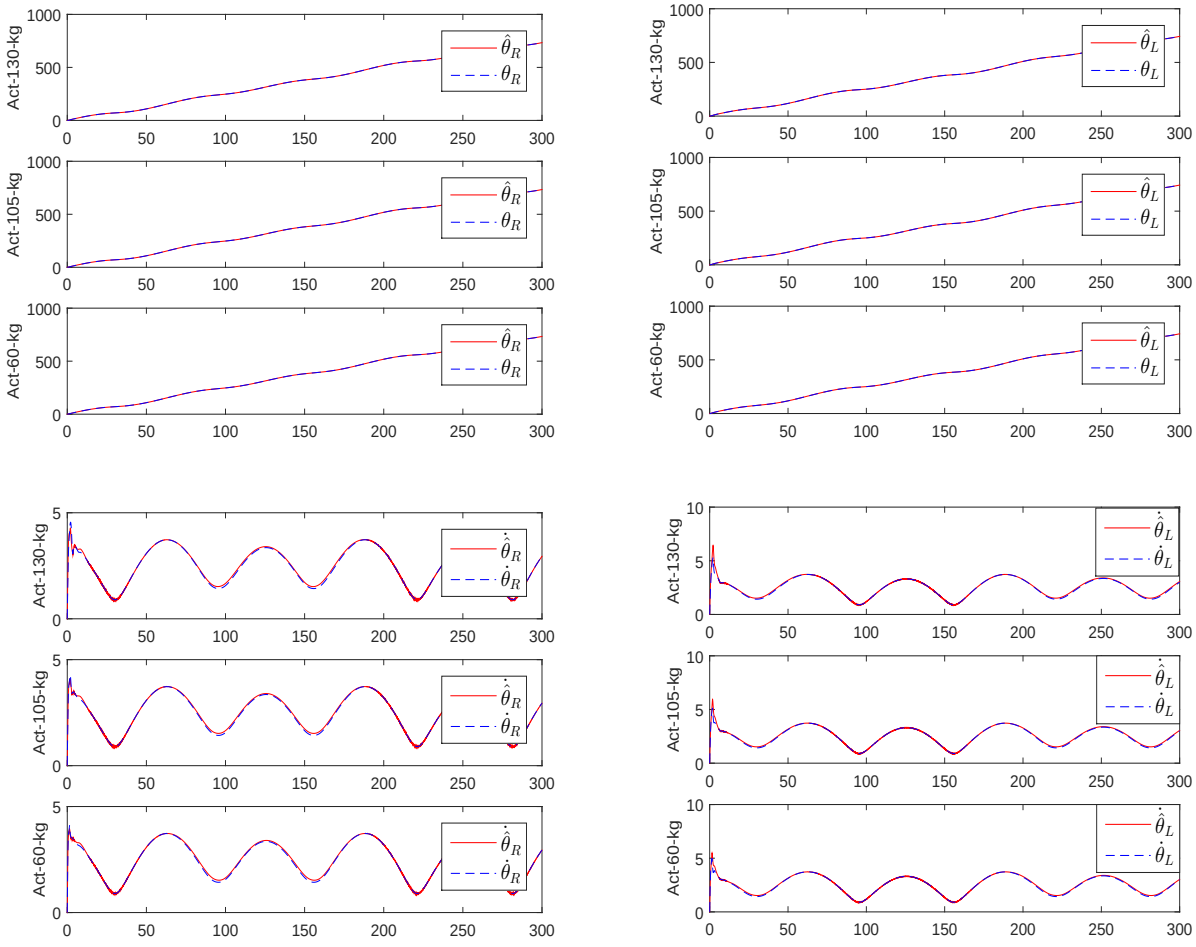

Figure 4.11: Figure eight SMO estimation results for wheel positions and velocities.

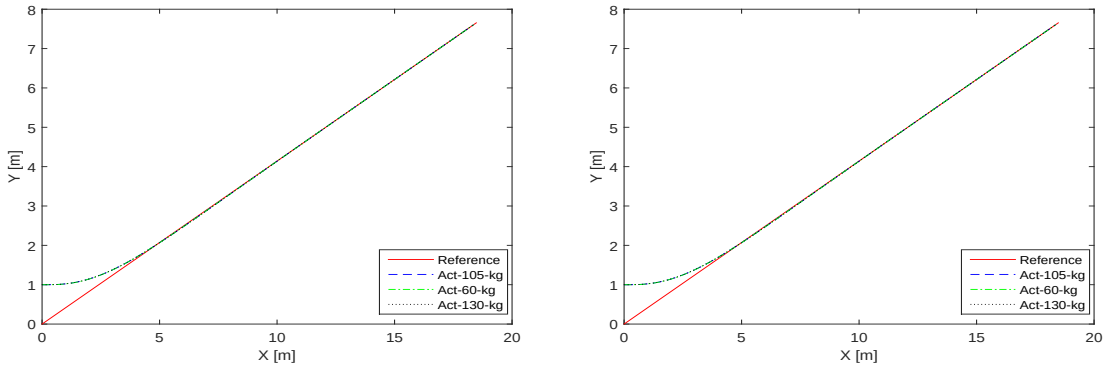

(a) (b)

Figure 4.12: Straight line tracking results for (a) PD controller and (b) SMC with HGO.

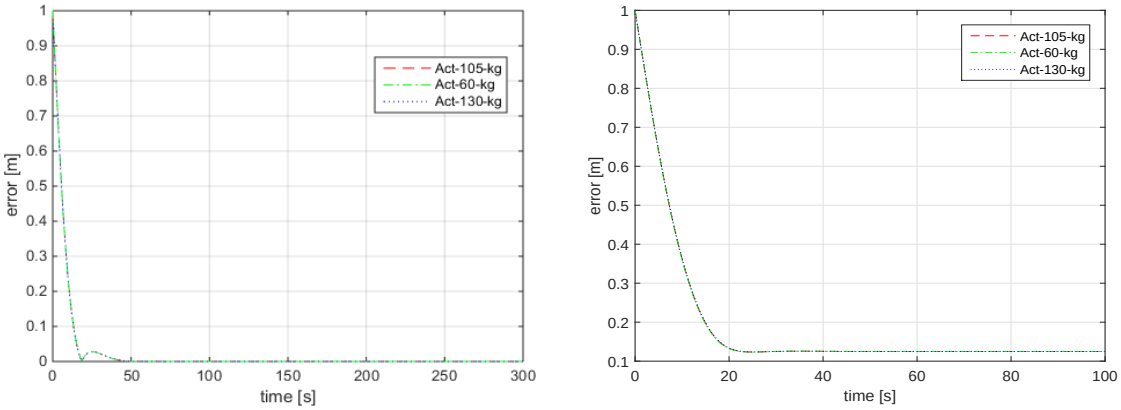

(a) (b)

Figure 4.13: Straight line tracking errors for (a) PD controller and (b) SMC with HGO.

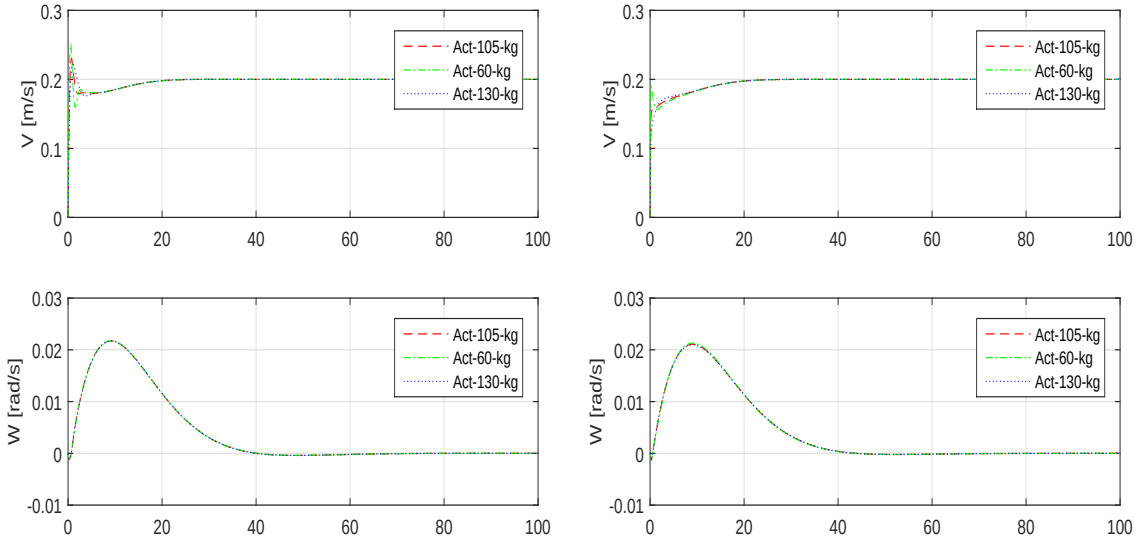

Figure 4.14: Straight line velocities for (a) PD controller and (b) SMC with HGO.

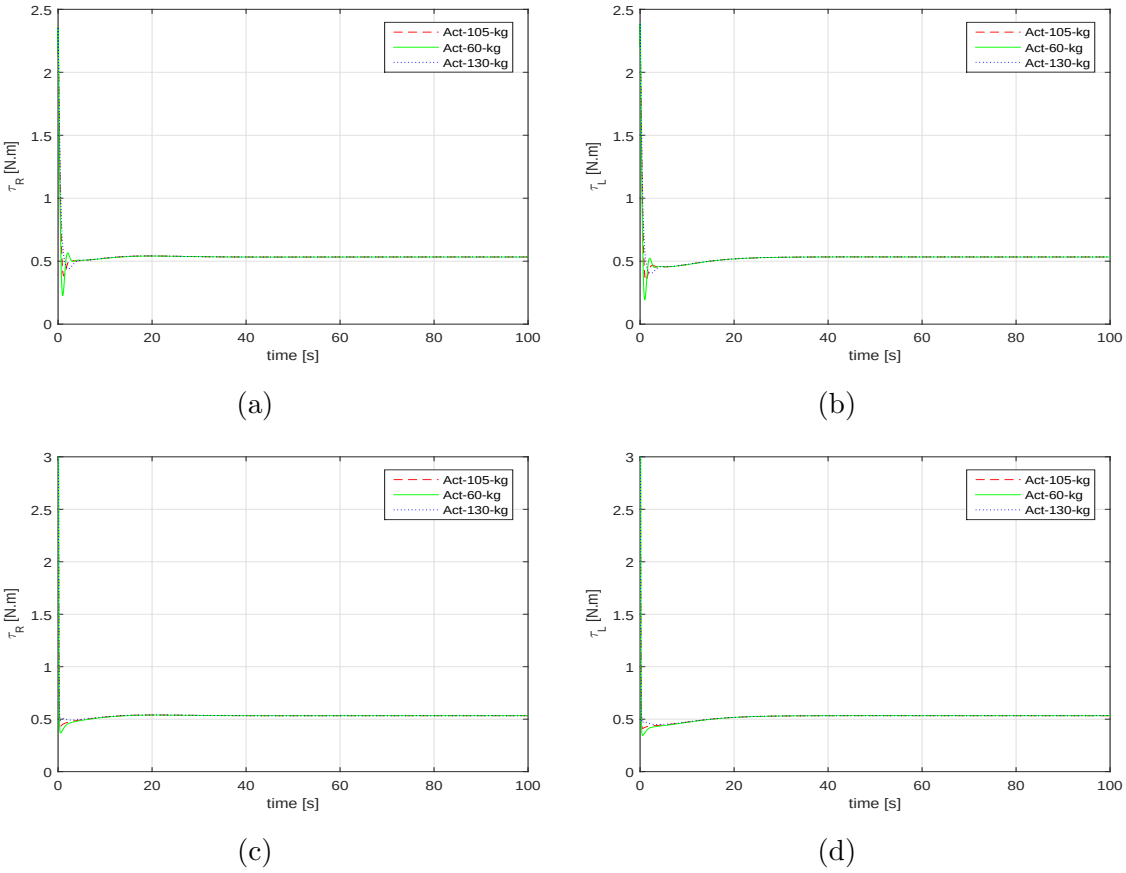

Figure 4.15: Straight line control torques of right and left wheels for (a,b) PD controller and (c,d) SMC with HGO.

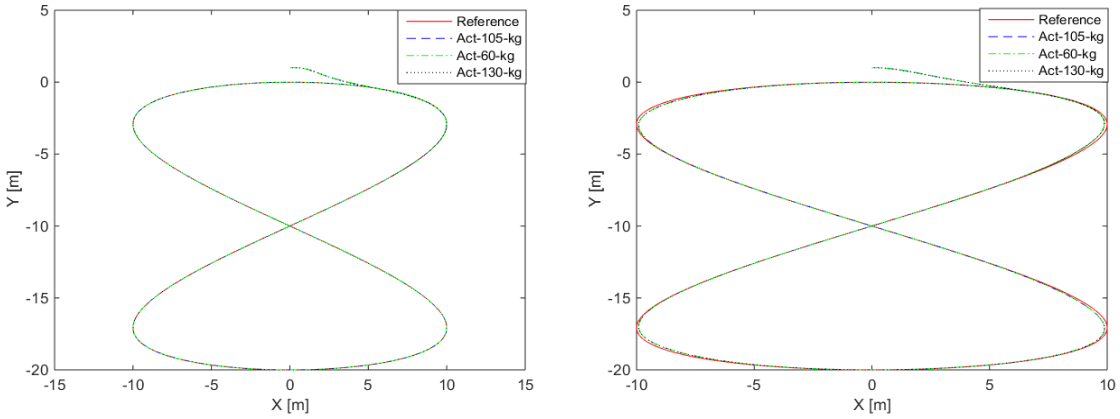

(a) (b)

Figure 4.16: Figure eight tracking results for (a) PD controller and (b) SMC with HGO.

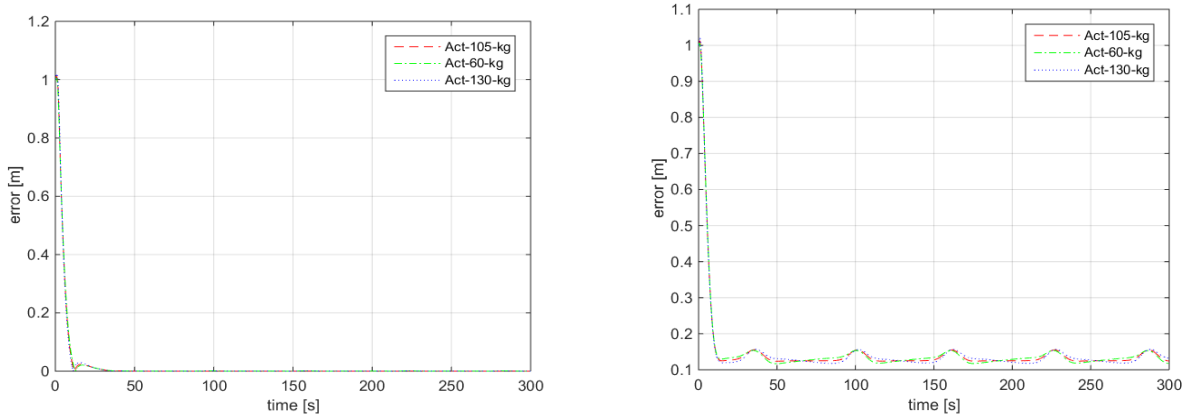

(a) (b)

Figure 4.17: Figure eight tracking errors for (a) PD controller and (b) SMC with HGO.

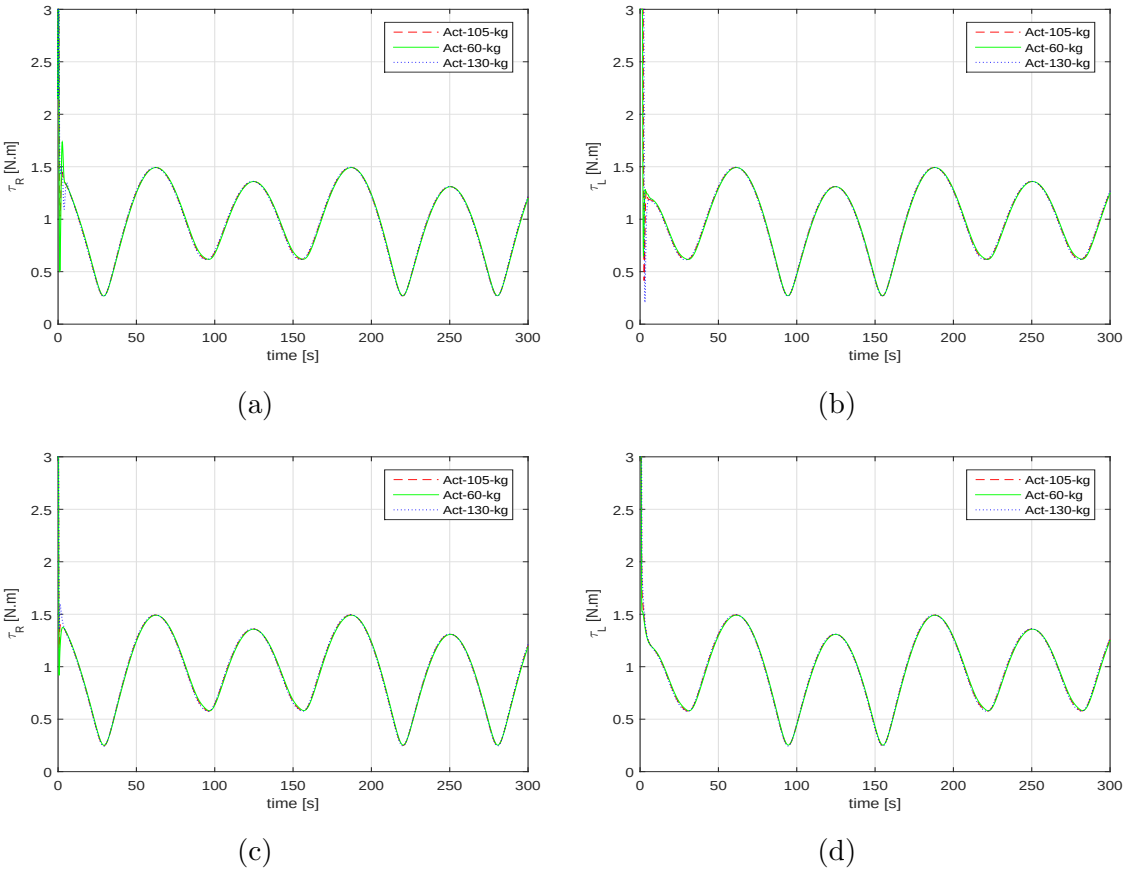

Figure 4.18: Figure eight control torques of right and left wheels for (a,b) PD controller and (c,d) SMC with HGO.

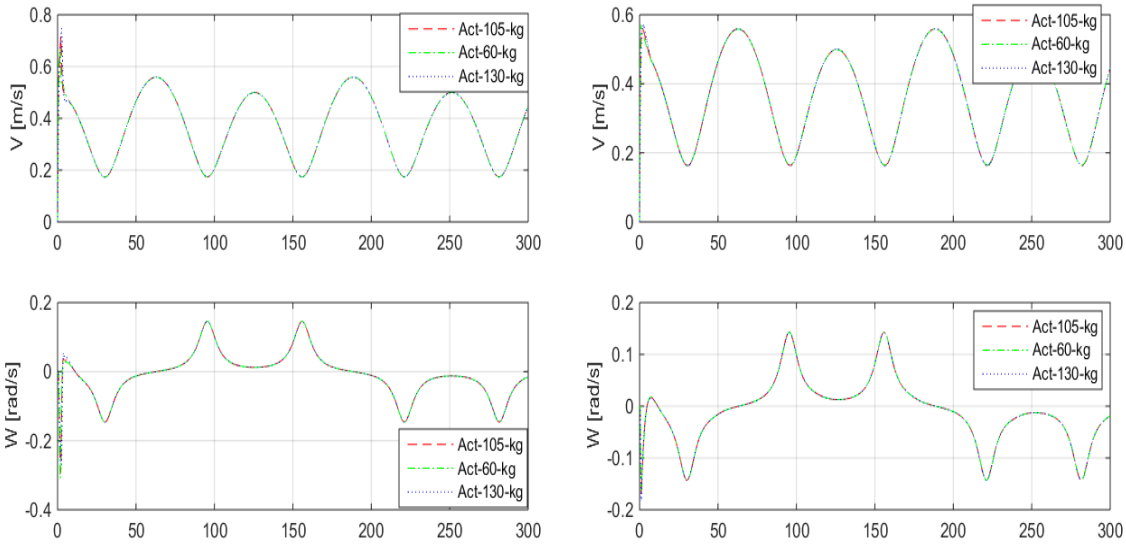

(a) (b)

Figure 4.19: Figure eight velocities for (a) PD controller and (b) SMC with HGO.

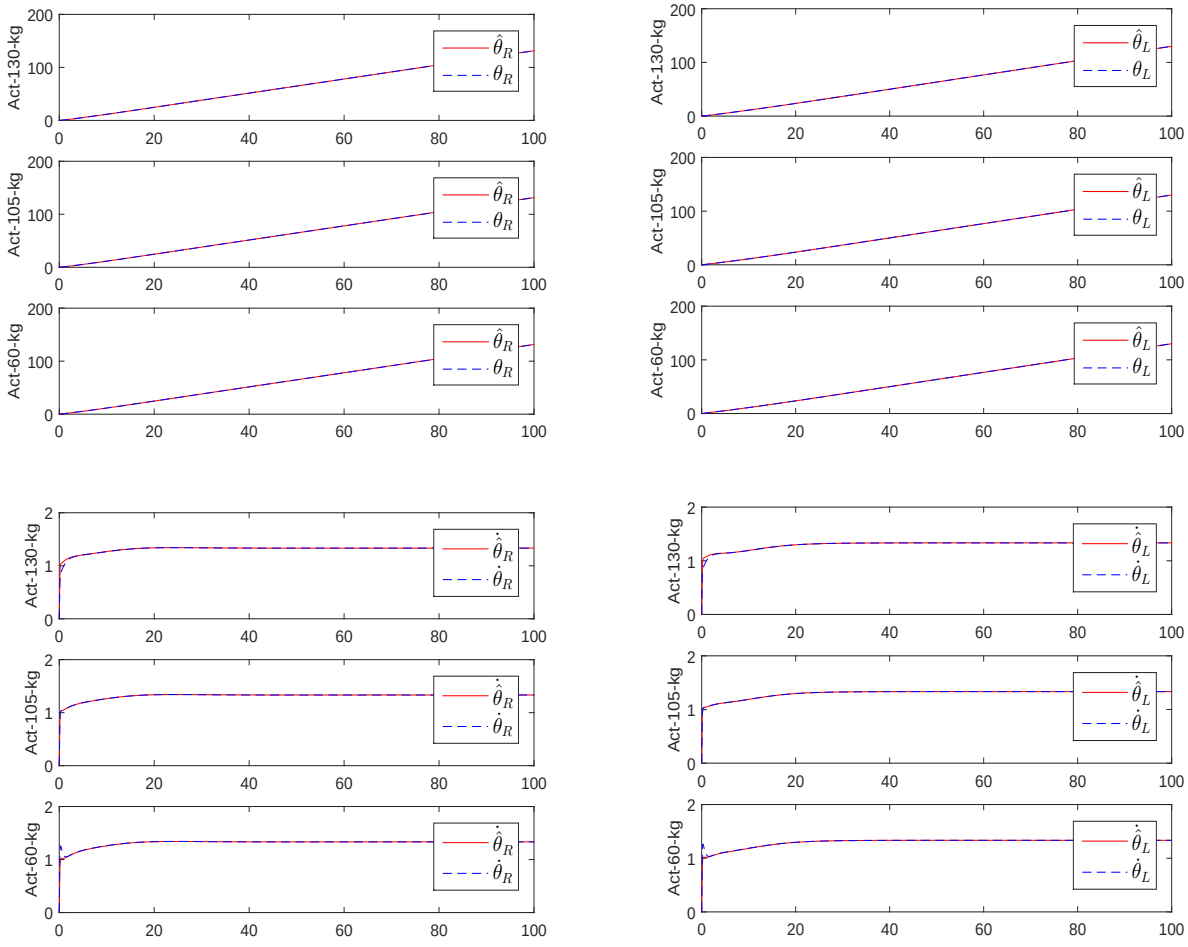

Figure 4.20: Straight line HGO estimation results for wheel positions and velocities.

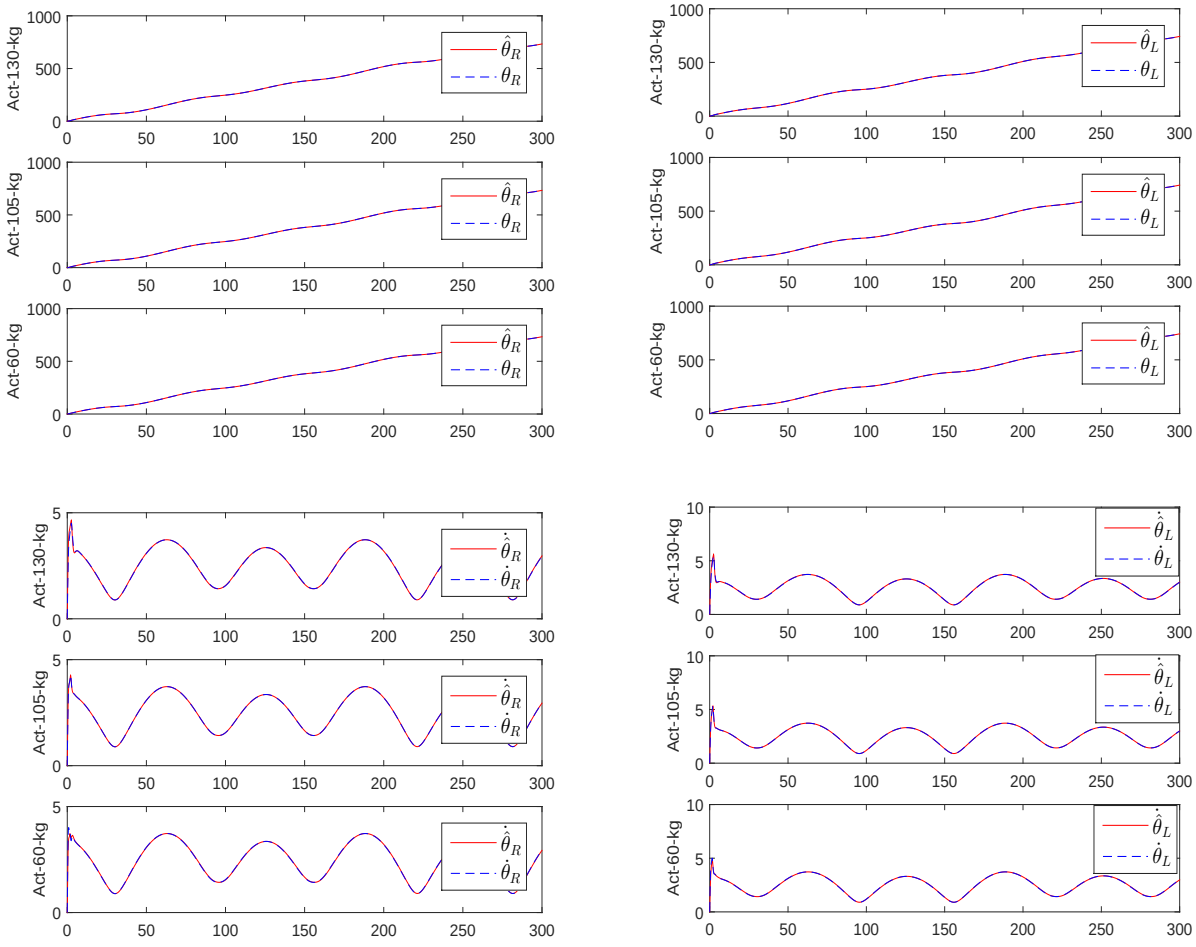

Figure 4.21: Figure eight HGO estimation results for wheel positions and velocities.

Chapter 5

Parameter Estimation and Adaptive Redesign

In this chapter, human mass effect and CG shifts are considered as unknown since they change according to the users. In this regard, how parameter changes effect on the system is examined. After that, parameter estimation steps are determined. First, a parametric models are defined based on the system dynamics, then estimation models and estimation errors are written. Adaptive versions of PD control scheme and SMC scheme are designed regarding the parameter estimates. Overall system is illustrated in Fig. 5.1.

5.1 Parameter Uncertainty Effects

In this section, the effect of parameter changes are presented. The used backstepping control scheme guarantees the stability of the system for any positive constant value of K_x, K_y, and K_α. The total mass of the i-walker support frame with all hardware is represented as a point mass at the distance of 45 cm from the point A. The i-walker itself has the mass of 20 kg and the capability of carrying 130 kg.

We make some assumptions to choose optimal control parameters. The vertical components of the user applied forces on the i-walker handles are assumed to be equal, and

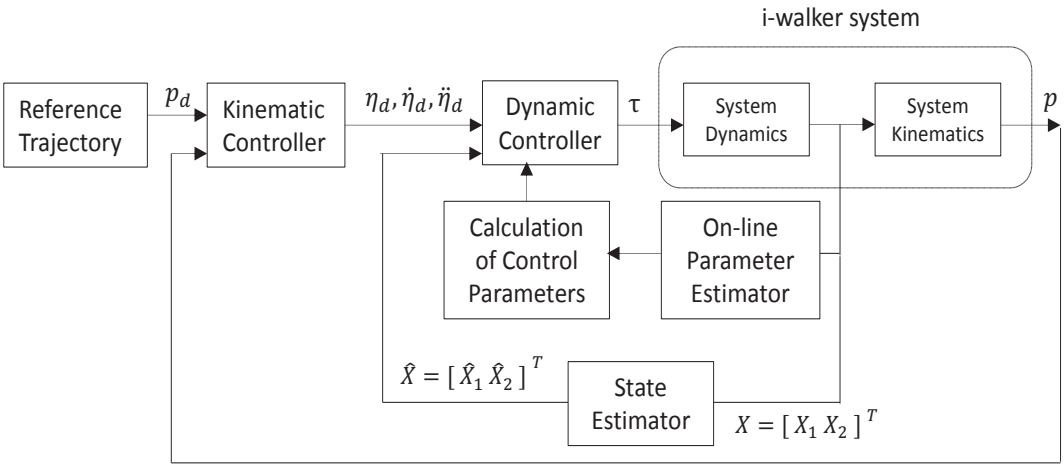

Figure 5.1: Overall system block diagram.

thus the total vertical force is applied to the point A, in the middle of rear wheels axis. This user applied force is considered as extra load for the i-walker dynamics. We consider that the mass of the i-walker with human, m_c, highly depends on the mass and the body posture of the user and affects the distance of CG from the point A, d, and total rotational inertia of the i-walker, I, according to the following two equations in (2.8),

$$m = m_c + 2m_w,$$

$$I = I_c + m_c d^2 + 2m_w L^2 + 2I_m.$$

However the linear increase in the value of m_c causes the nonlinear decrease in d and I. These changes suppress the effect of each other, and thus C matrix is not affected by m_c and d. This change is illustrated in Fig. 5.2. The nominal total mass of the i-walker is chosen as 36 kg for the controller. Upper and lower limits for the i-walker system are decided regarding nominal mass as 46, 26, respectively. Moreover, when looking at the eigenvalues of $\bar{M}$ matrix, eigenvalues has an inconsiderable change in CG shifts and load changes as shown in Fig. 5.3.

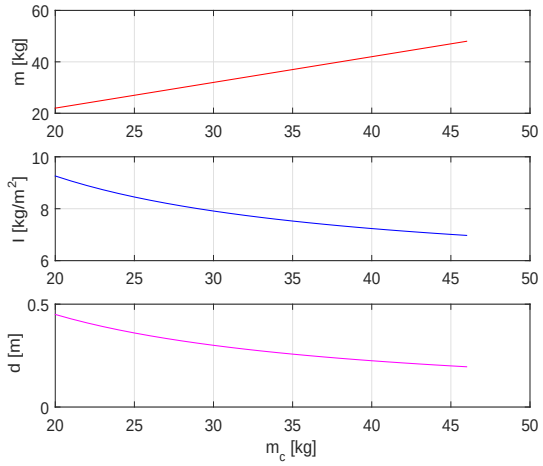

Figure 5.2: Parameter changes.

5.2 Adaptive Redesign

In this section, an adaptive control algorithm is developed for the i-walker based on the parameter identification [43]. (2.10) is rewritten as

$$\bar{M}\ddot{\eta} + \bar{C}\dot{\eta} = \tau, \tag{5.1}$$

where

$$\bar{M} = \begin{bmatrix} \frac{mr^2}{4} + \frac{Ir^2}{4L^2} + I_w & \frac{mr^2}{4} - \frac{Ir^2}{4L^2} \\ \frac{mr^2}{4} - \frac{Ir^2}{4L^2} & \frac{mr^2}{4} + \frac{Ir^2}{4L^2} + I_w \end{bmatrix},$$

$$\bar{C} = \begin{bmatrix} b_m & m_c\frac{r^2 d}{2L}\dot{\alpha} \\ -m_c\frac{r^2 d}{2L}\dot{\alpha} & b_m \end{bmatrix}.$$

In this study, we have two unknown parameters, m_c and d. In order to estimate these parameters, parameter identification steps are implemented.

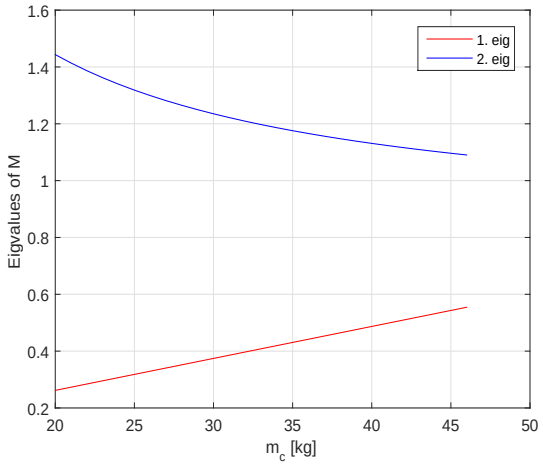

Figure 5.3: Eigenvalues of $\bar{M}$.

5.2.1 Parametric model

First step of the parameter identification is to define a parametric model. Let each component of $\bar{M}$ and $\bar{C}$ matrices be the unknown parameters of the system.

$$\begin{aligned} \theta_1^* &= \frac{mr^2}{4} + \frac{Ir^2}{4L^2} + I_w, \\ \theta_2^* &= \frac{mr^2}{4} - \frac{Ir^2}{4L^2}, \\ \theta_3^* &= m_c \frac{r^2 d}{2L}. \end{aligned} \tag{5.2}$$

The dynamic equation (2.10) is rewritten considering the definition in (5.2) as

$$\begin{bmatrix} \theta_1^* & \theta_2^* \\ \theta_2^* & \theta_1^* \end{bmatrix} \begin{bmatrix} \ddot{\theta}_R \\ \ddot{\theta}_L \end{bmatrix} + \begin{bmatrix} b_m & \theta_3^* \dot{\alpha} \\ -\theta_3^* \dot{\alpha} & b_m \end{bmatrix} \begin{bmatrix} \dot{\theta}_R \\ \dot{\theta}_L \end{bmatrix} = \begin{bmatrix} \tau_R & 0 \\ 0 & \tau_L \end{bmatrix} \tag{5.3}$$

Using the equation above, each row of the matrix is considered as a separate equation.

$$\begin{aligned} \theta_1^* \ddot{\theta}_R + \theta_2^* \ddot{\theta}_L + b_m \dot{\theta}_R + \theta_3^* \dot{\theta}_L \dot{\alpha} &= \tau_R, \\ \theta_2^* \ddot{\theta}_R + \theta_1^* \ddot{\theta}_L + b_m \dot{\theta}_L - \theta_3^* \dot{\theta}_R \dot{\alpha} &= \tau_L. \end{aligned} \tag{5.4}$$

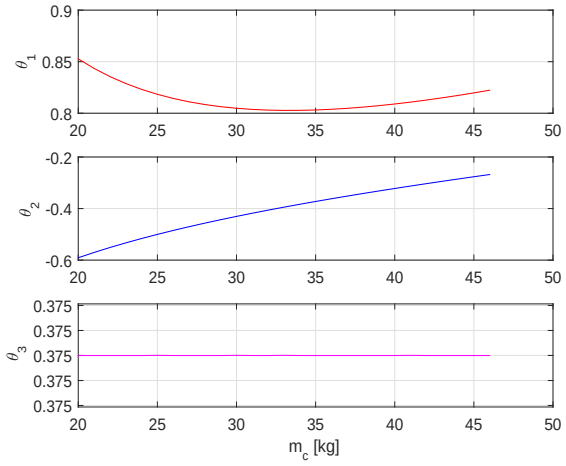

Figure 5.4: Parameter changes

θ_R and θ_L are available for measurement, $\dot{\theta}_R$ and $\dot{\theta}_L$ are estimated by observers. The second derivations can be obtained via estimated values. These equations can be rewritten by collecting all unknown parameters in one side.

$$\begin{aligned} \theta_1^*\ddot{\theta}_R + \theta_2^*\ddot{\theta}_L + \theta_3^*\dot{\hat{\theta}}_L\dot{\alpha} &= \tau_R - b_m\dot{\hat{\theta}}_R \\ \theta_2^*\ddot{\theta}_R + \theta_1^*\ddot{\theta}_L - \theta_3^*\dot{\hat{\theta}}_R\dot{\alpha} &= \tau_L - b_m\dot{\hat{\theta}}_L \end{aligned} \tag{5.5}$$

Unknown parameters are collected into a vector, then static parametric models (SPM) are formed as follows:

$$z_1 = \theta^{*^T}\phi_1 = \tau_R - b_m\dot{\hat{\theta}}_R, \tag{5.6}$$

$$z_2 = \theta^{*^T}\phi_2 = \tau_L - b_m\dot{\hat{\theta}}_L, \tag{5.7}$$

$$\theta^* = \begin{bmatrix} \theta_1^* & \theta_2^* & \theta_3^* \end{bmatrix}^T, \tag{5.8}$$

$$\begin{aligned} \phi_1 &= \begin{bmatrix} \ddot{\theta}_R & \ddot{\theta}_L & \dot{\alpha}\dot{\hat{\theta}}_L \end{bmatrix}^T, \\ \phi_2 &= \begin{bmatrix} \ddot{\theta}_L & \ddot{\theta}_R & -\dot{\alpha}\dot{\hat{\theta}}_R \end{bmatrix}^T, \end{aligned} \tag{5.9}$$

where $z_1, z_2 \in \mathbb{R}$ and $\phi_1, \phi_2 \in \mathbb{R}^n$ are signals available for measurement, and $\theta^* \epsilon \mathbb{R}^n$ is the vector with all unknown parameters. For the parameter estimation of the system, we examine the parameter values for the changing m_c as seen in Fig. 5.4. The total change in all states is small. These values could be used to set bound our estimates which may decrease the convergence time of the actual values.

5.2.2 Adaptive Algorithm

After having a suitable parametric model for the system, now estimation model and error can be obtained. Least-squares algorithm is implemented to the system as adaptive law.

Estimation Model and Estimation Error

Estimation models are designed in the same form as the parametric models.

$$\begin{aligned} \hat{z}_1 &= \theta^T \phi_1, \\ \hat{z}_2 &= \theta^T \phi_2, \end{aligned} \tag{5.10}$$

$$\theta = \begin{bmatrix} \theta_1 & \theta_2 & \theta_3 \end{bmatrix}^T,$$

where $\hat{z}_1$, $\hat{z}_2$, θ are the estimation of z_1, z_2, θ^*, respectively. Estimation errors $(\varepsilon_1, \varepsilon_2)$ are the difference between the outputs of the models that have been presented above.

$$\begin{aligned} \varepsilon_1 &= \frac{z_1 - \hat{z}_1}{m_{s_1}^2} = \frac{-\tilde{\theta}^T \phi_1}{m_{s_1}^2}, \quad m_{s_1}^2 = 1 + \alpha_1 \phi_1^T \phi_1, \quad \alpha_1 \geq 1 \\ \varepsilon_2 &= \frac{z_2 - \hat{z}_2}{m_{s_2}^2} = \frac{-\tilde{\theta}^T \phi_2}{m_{s_2}^2}, \quad m_{s_2}^2 = 1 + \alpha_2 \phi_2^T \phi_2, \quad \alpha_2 \geq 1 \end{aligned} \tag{5.11}$$

where $\tilde{\theta} = \theta - \theta^*$.

Adaptive Law

In this study, Least-squares algorithm with forgetting factor are used for the parametric model.

Least - Squares Algorithm : LS Algorithm is simply used to analyse the unknown parameters in static parametric model. Recursive LS algorithm with forgetting factor can be written as

$$\begin{aligned}
\dot{\theta} &= P_1\varepsilon_1\phi_1 + P_2\varepsilon_2\phi_2, \quad \theta(0) = \theta_0, \\
\dot{P}_1 &= \beta P_1 - P_1\frac{\phi_1\phi_1^T}{m_{s_1}^2}P_1, \quad P_1(0) = P_{1_0} = Q_0^{-1}, \\
\dot{P}_2 &= \beta P_2 - P_2\frac{\phi_2\phi_2^T}{m_{s_2}^2}P_2, \quad P_2(0) = P_{2_0} = Q_0^{-1},
\end{aligned} \tag{5.12}$$

where P_1, P_2 are covariance matrices, $Q_0 = Q_0^T > 0$ and $\phi_1\phi_1^T, \phi_2\phi_2^T$ are positive definite.

5.3 Adaptive Proportional Derivative Control

In order to form the adaptive PD control scheme, the output feedback control law (4.8) is considered in this section. Substituting (4.8) in (3.13), adaptive PD control scheme can be designed as

$$\tau = \hat{\bar{M}}(\ddot{\eta}_d - \hat{u}) + \hat{\bar{C}}\hat{X}_2, \tag{5.13}$$

where $\hat{\bar{M}}$, $\hat{\bar{C}}$ are the estimates of $\bar{M}$, $\bar{C}$. The closed loop adaptive PD control system is designed by (4.8), (5.13).

5.4 Adaptive Sliding Mode Control

After having estimated state and parameters, now an adaptive SMC can be designed. Consider the system dynamics in (3.20) and output feedback SMC in Chapter 4. Adaptive SMC scheme can be redesigned, replacing $\bar{M}$, $\bar{C}$ with their estimates $\hat{\bar{M}}$, $\hat{\bar{C}}$.

$$\tau_0 = -\hat{\bar{M}}\left(-\hat{\bar{M}}^{-1}\hat{\bar{C}}\left(\hat{X}_2\right)\hat{X}_2 - \ddot{\eta}_d - \lambda\dot{\hat{E}}_2\right), \tag{5.14}$$

$$\tau = \tau_0 - \hat{\bar{M}}k_1 sgn(s). \tag{5.15}$$

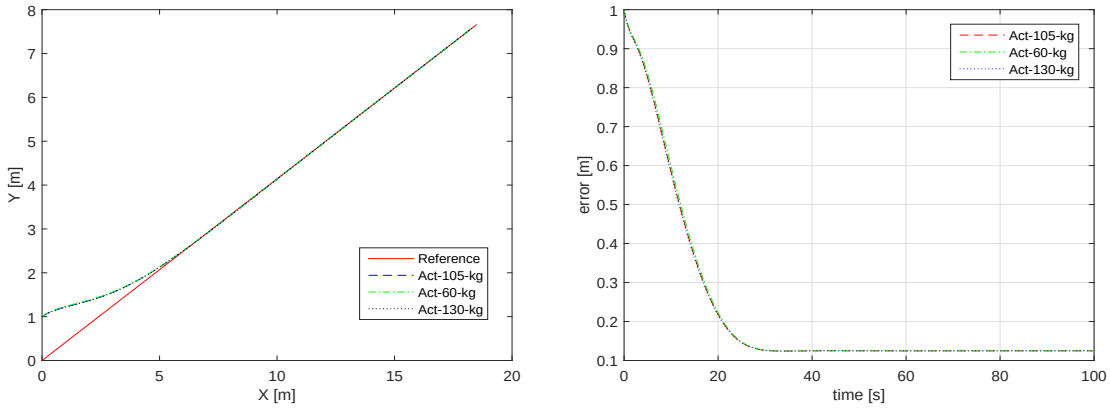

(a) Trajectory tracking.

(b) Tracking error.

Figure 5.5: Straight line tracking results with parameter estimates.

5.5 Simulations

In this section, simulation results are presented for overall system with estimates of state and parameters. In the previous Chapter, we presented the effectiveness of the proposed controllers and observers. Therefore, PD control scheme and SMC scheme can be used with either SMO or HGO. In this section, we simulated PD control scheme with HGO for straight path and SMC scheme with SMO for figure eight path.

Case 1: The straight path is defined as $x_d = 0.25t\cos\left(\frac{\pi}{8}\right)$, $y_d = 0.25t\sin\left(\frac{\pi}{8}\right)$, $\alpha_d = \pi/8$ and the initial conditions are given the same as in Chapter 3, $(x_0, y_0, \alpha_0) = (0, 1, 0)$.

Simulation results for the straight line trajectory are plotted in Figs. 5.5-5.8. Fig. 5.5 presents the tracking results in (x,y) plane, Fig. 5.6 displays the control torques, Figs. 5.7 shows the velocities, Fig. 5.8 plots the parameter estimation results.

Case 2: The figure eight trajectory is defined as $x_d = 10sin(0.05t)$ and $y_d = 10cos(0.025t) - 10$. The initial conditions for figure eight are chosen as $(x_0, y_0, \alpha_0) = (1, 0.01, 0)$.

Similar to straight line, figure "8" simulations are given in Figs. 5.9-5.12. Fig. 5.9 shows the tracking results, Fig. 5.10 displays the control torques, Figs. 5.11 presents the

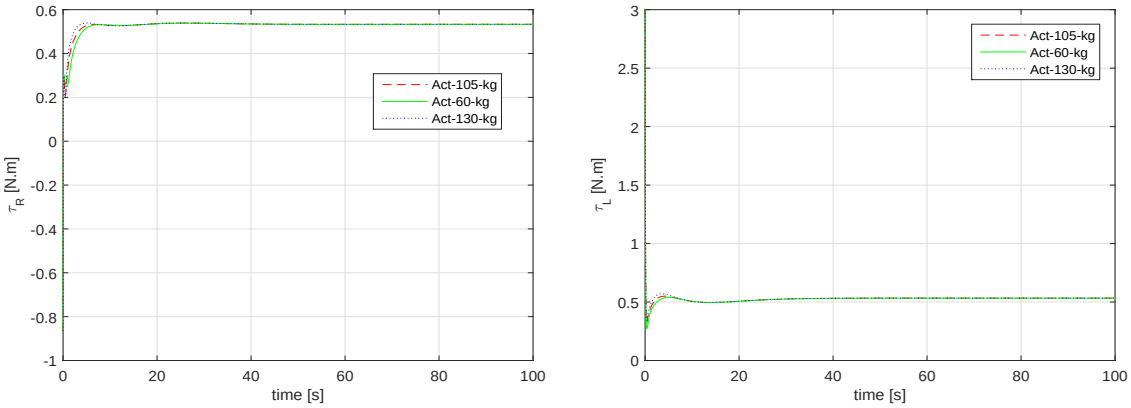

Figure 5.6: Straight line control torques for PD controller and SMC.

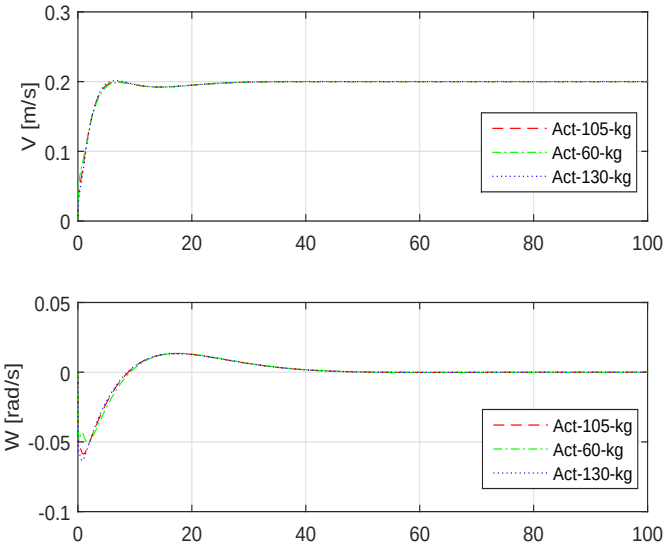

Figure 5.7: Straight line velocity results.

velocities, Fig. 5.12 plots parameter estimation results.

The simulation results demonstrate that the i-walker system follows the desired trajectory with estimated states and parameters, tracking errors converge to zero in time. The proposed control schemes, observers are effective for path tracking. System has become

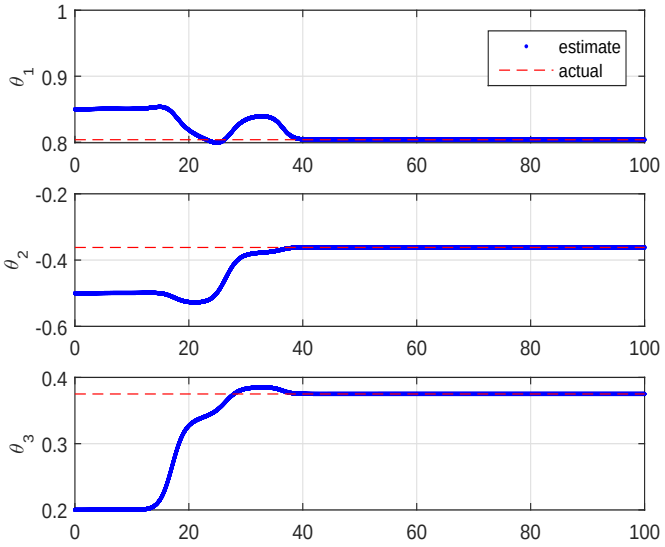

Figure 5.8: Straight line parameter estimation results.

robust to CG shifts and load changes.

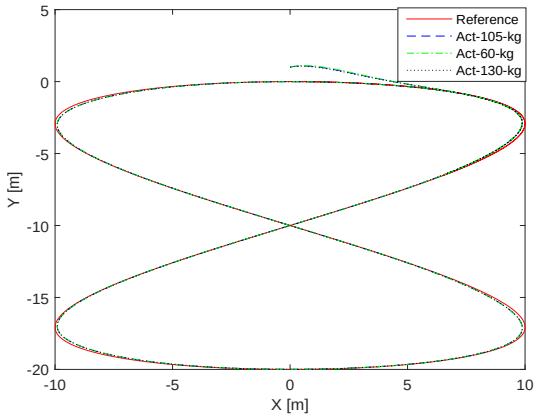

(a) Trajectory tracking.

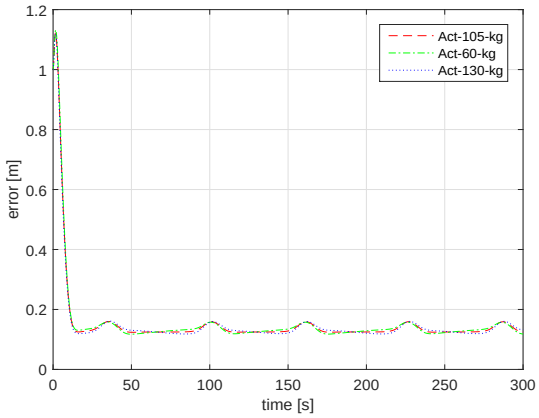

(b) Tracking error.

Figure 5.9: Figure eight tracking results with parameter estimates.

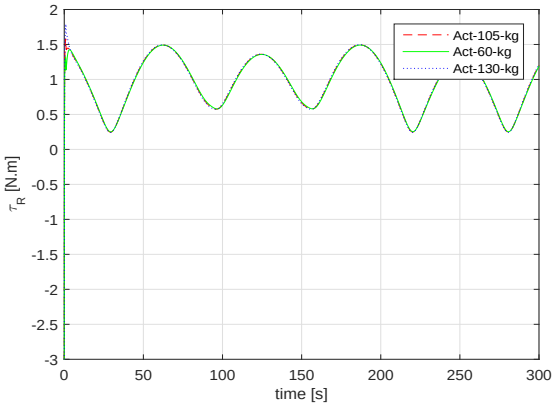

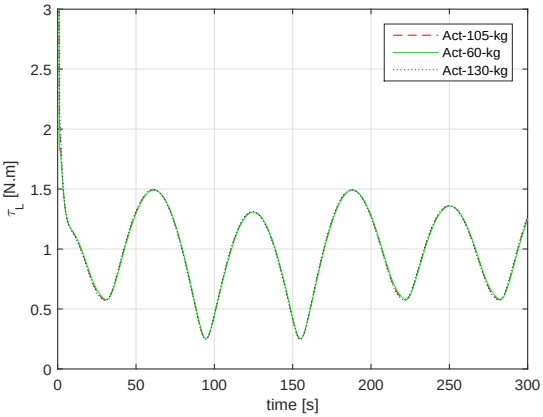

Figure 5.10: Figure eight control torques.

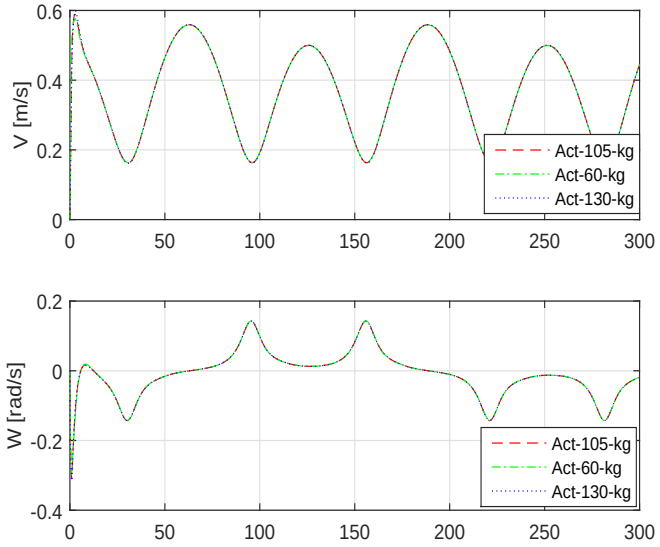

Figure 5.11: Figure eight velocity results.

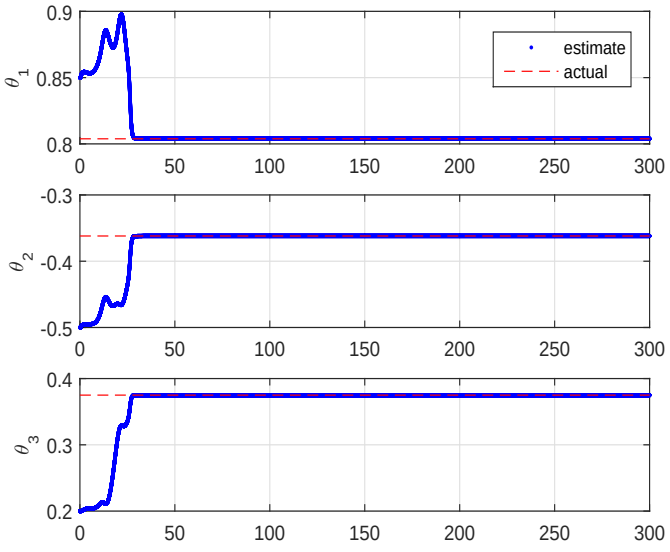

Figure 5.12: Figure eight parameter estimation results.

Chapter 6

Conclusion and Future Work

This thesis focuses on tracking desired trajectories of i-walkers considering safe motion. In this regard, a two-part control problem is discussed. In the high level control part, a kinematic controller based on integrator backstepping is designed that produces the desired velocities for the i-walker system. In the low level control part, feedback linearization of the system dynamics are considered to apply the state feedback controllers for path tracking and combined with two dynamic controllers, PD controller and SMC, respectively to apply the control torques. Stability analysis of the proposed control schemes is provided. A set of simulations are conducted for different motion characteristics such as curved and straight. The simulation results demonstrate the effectiveness of the proposed control schemes for minimizing the tracking errors. In order to do so, all states are considered as known. However, in actual case, noise problems must be taken into consideration due to the velocity measurements. To this end, state estimators, SMO and HGO, are designed to estimate wheel velocities. Then, output feedback PD and SMC schemes are designed utilizing estimated state. Tracking performances are illustrated via simulations. Simulations show that the i-walker system tracks the reference path with designed observers and control schemes. Lastly, human mass effect and CG shift are considered as unknown, and hence parameter identification steps are examined. An appropriate parametric model is formed, then estimation model and error is defined. Adaptive PD control and SMC are designed based on parameter estimates. Estimation results are demonstrated using simulations.

Designed control schemes, state and parameter estimators are well-achieved. Furthermore, non-adaptive control design itself achieves the tracking task since the parameter changes inconsiderably effects the system. Even if the parameter estimates and adaptive control scheme results are good enough, non-adaptive one itself is robust to CG shifts and load changes.

Future work will focus on the real life applications and instrumentation. Designed observers and control schemes will be applying to an i-walker system in experiment. Instrumentation will also be performed since the selection of sensors and actuators is key to obtain appropriate signals from the i-walker system.

Bibliography

[1] P. F. Cipriano, C. A. Gassert, and L. B. Bolton "Smart technology, enduring solutions: technology solutions can make nursing care safer and more efficient," *American Academy of Nursing*, vol. 22, no. 4, 2008

[2] X. Chen, Y. Jia, F. Matsuno, "Tracking control of nonholonomic mobile robots with velocity and acceleration constraints," *American Control Conference*, pp. 880-884, Portland, Jun. 2014

[3] M. Saida, Y. Hirata, K. Kosuge, "Motion control of passive mobile robot consisting of casters with servo brakes," *IEEE/RSJ International Conference on Intelligent Robot and Systems*, St. Louis, USA, 2009

[4] C. Ko, K. Young, Y. Huang, S. Agrawal, "Active and passive control of walk-assist robot for outdoor guidance," *IEEE/ASME Transactions on Mechatronics*, vol. 18, no. 3, 2013

[5] R. P. Tan, S. Y. Wang, Y. L. Jiang, K. Ishida, M. G. Fujie, "Motion control of omni-directional walker for walking support," *IEEE/ICME International Conference on Complex Medical Engineering*, Harbin, China, 2011

[6] S. Suzuki, Y. Hirata, K. Kosuge, H. Onodera, "Motion support during the swing phase using cooperative walking support system," *International Journal of Advanced Robotics*, vol. 27, no. 17, pp. 1337-1349, 2013

[7] R. Millan, F. Galan, D. Vanhooydonck, E. Lew, J. Philips, M. Nuttin, "Asynchronous non-invasive brain-actuated control of an intelligent wheelchair," *31st Annual International Conference of the IEEE EMBS*, Minneapolis, Sep. 2009

[8] C. Barrué, R. Annicchiarico, U. Cortés, A. Martínez-Velasco, E. X. Martín, F. Campana, C. Caltagirone, "The i-Walker: an intelligent pedestrian mobility aid," *Computational Intelligence in Healthcare 4 Studies in Computational Intelligence*, vol. 309, pp. 103-123, 2010

[9] T. Carlson, and Y. Demiris, "Collaborative control for a robotic wheelchair: evaluation of performance, attention, and workload," *IEEE Transactions On Systems, Man, and Cybernetics Part B: Cybernetics*, vol. 42, no. 3, Jun. 2012

[10] Y. Hirata, A. Hara, K. Kosuge, "Motion control of passive intelligent walker using servo brakes," *IEEE Transactions on Robotics*, vol. 23, no. 5, pp. 981-990, Oct. 2007

[11] R. Meyer, F. Just, R. A. DeCarlo, M. Zefran, M. Oishi, "Notch filter and MPC for powered wheelchair operation under Parkinson's Tremor," *American Control Conference*, Portland, Jun. 2014

[12] Y. Wang, S. Wang, R. P. Tan, Y. L. Jiang, "Adaptive control method for path tracking of wheeled mobile robot considering parameter changes," *IEEE International Journal of Advanced Mechatronic Systems*, vol. 4, no. 1, 2012

[13] Y. Hirata, C. Oscar Jr, A. Hara, and K. Kosuge, "Human adaptive motion control of active and passive type walking support system," *IEEE Workshop on Advanced Robotics and its Social Impacts*, pp. 139-144, Jun. 2005

[14] C.H. Ko, K. Young, Y. Huang, and S.K. Agrawal, "Active and passive control of walk-assist robot for outdoor guidance," *IEEE/ASME Transactions on Mechatronics*, vol. 18, no. 3, pp. 1211-1220, Jun. 2013

[15] Y. Hirata, A. Muraki, and K. Kosuge, "Motion control of intelligent walker based on renew of estimation parameters for user state," *IEEE/RSJ International Conference on Intelligent Robots and Systems*, pp. 1050-1055, Oct. 2006

[16] A. Silva Jr., and F. Sup, "Design and control of a two-wheeled robotic walker for balance enhancement," *IEEE International Conference on Rehabilitation Robotics*, 2013

[17] R.P. Tan, S.Y. Wang, Y.L. Jiang, K. Ishida, and M.G. Fujie, "Motion Control of Omni-Directional Walker for Walking Support," *IEEE/ICME International Conference on Complex Medical Engineering*, pp. 633-636, Harbin, May 2011

[18] B. Zhoua, J. Han, X. Dai, "Backstepping Based Global Exponential Stabilization of a Tracked Mobile Robot with Slipping Perturbation," *Journal of Bionic Engineering*, vol. 8, issue 1, pp. 69–76, 2011

[19] R.P. Tan, S.Y. Wang, Y.L. Jiang, T. Chai, K. Ishida, and M.G. Fujie, "Adaptive Controller for Omni-Directional Walker: Improvement of Dynamic Model," *IEEE International Conference on Mechatronics and Automation*, pp. 325-330, Beijing, Aug. 2011

[20] Y.N. Wang, S.Y. Wang, R.P. Tan, Y.L. Jiang, K. Ishida, and M.G. Fujie, "Adaptive Control Method for a Walking Support Machine Considering Center of Gravity Shifts and Load Changes," *IEEE International Conference on Advanced Mechatronic Systems*, pp. 684-689, Tokyo, Sep. 2012

[21] A. Zhang, J. She, X. Lai, M. Wu, J. Qiu, and X. Chen "Robust Tracking Control of Robot Manipulators Using Only Joint Position Measurements," *Mathematical Problems in Engineering* vol. 2013, 2013

[22] J. J. Slotine, J. K. Hedrick, and E. A. Misawa, "On sliding observers for nonlinear systems," *Journal of Dynamic Systems, Measurement, and Control*, vol. 109/245, Sep. 1987

[23] M. Krstic, and P. V. Kokotovic, "Observer based schemes for adaptive nonlinear state feedback control," *International Journal of Control*, vol. 59, no.6, pp. 1373-1381, 1994

[24] G. Bastin, and M. R. Gevers, "Stable adaptive observers for nonlinear time varying systems," *IEEE Transactions on Automatic Control*, vol. 33, no. 7, pp. 650-658, Jul. 1988

[25] M. M. Arefi, J. Zarei, and H. R. Karimi, "Observer-based adaptive stabilization of a class of uncertain nonlinear systems," *Systems Science & Control Engineering: An Open Access Journal*, vol. 2, pp. 362-367, 2014

[26] C. C. de WlT, and J.-J. E. Slotine, "Sliding observers for robot manipulators," *Automatica*, vol. 27, no. 5, pp. 859-864, 1991

[27] Y. Liu, "Robust adaptive observer for nonlinear systems with unmodeled dynamics," *Automatica*, vol. 45, no. 8, pp. 1891-1895, Aug. 2009

[28] J.-J. E. Slotine, and S. S. Sastry, "Tracking control of non-linear systems using sliding surfaces with application to robot manipulators," *American Control Conference* pp. 132-135, San Francisco, Jun. 1983

[29] J.C.Doyle and G.Stein, "Robustness with Observers," *IEEE Transactions on Automatic Control*, AC-24, no. 4, pp. 607-611, 1979

[30] I.R.Petersen and C.V.Holot, "High gain observers applied to problems in disturbance attenuation, H-infinity optimization and the stabilization of uncertain linear systems," *Proceedings of American Control Conference*, pp. 2490-2496, Jun. 1988

[31] H.K.Khalil and A.Saberi, "Adaptive stabilization of a class of nonlinear systems using high-gain feedback," *IEEE Transactions on Automatic Control*, AC-32, no. 11, pp. 1031-1035, 1987

[32] H. J. Sussmann, and P. V. Kokotovic, "The peaking phenomenon and the global stabilization of nonlinear systems," *IEEE Transactions on Automatic Control*, vol. 36, no. 4, pp. 424-440, Apr. 1991

[33] Fall Guys Research Lab, Research on falls and more, *http://fallguysresearchlab.com/for-patientsfamilies/*

[34] R. Fierro and F. L. Lewis, "Control of a nonholonomic mobile robot: Backstepping kinematics into dynamics," *Journal of Robotic Systems*, vol. 14, issue 3, pp. 149-163, Mar. 1997

[35] R. Fierro and F.L. Lewis, "Control of a Nonholonomic Mobile Robot: Backstepping Kinematics into Dynamics," *Proc. IEEE Conference on Decision and Control*, vol. 4, pp. 3805-3810, Dec. 1995

[36] M. Boukattaya, M. Jallouli, T. Damak, "On trajectory tracking control for nonholonomic mobile manipulators with dynamic uncertainties and external torque disturbances," *Robotics and Autonomous Systems* vol. 60, issue. 12, pp. 1640-1647, Dec. 2012

[37] F.L. Lewis, D.M. Dawson, and C.T. Abdallah, *Robot Manipulator Control Theory and Practice*, CRC Press, 2003

[38] J.J.E. Slotine and W. Li, *Applied Nonlinear Control*, Prentice-Hall, Englewood Cliff, New Jersey, 1991

[39] R. M. Murray, Z. Li and S. S. Sastry, *A Mathematical Introduction to Robotic Manipulation*, CRC Press, 1993

[40] J. Y. Tung, W. H. Gage, P. Poupart, W. E. Mcllroy, "Upper limb contributions to frontal plane balance control in rollator-assisted walking," *Assistive Technology: The Official Journal of RESNA*, 26:1, pp. 15-21, 2014

[41] H. K. Khalil and L. Praly, "High-gain observers in nonlinear feedback control," *International Journal of Robust and Nonlinear Control*, vol. 24, issue 6, pp. 993–1015, Apr. 2014

[42] H. K. Khalil, *Nonlinear Systems Third Edition*, Prentice Hall, 2002

[43] P.Ioannou and B.Fidan, *Adaptive Control Tutorial*, Society for Industrial and Applied Mathematics, Philadelphia, 2006